LBL-24563
Preprint

Lawrence Berkeley Laboratory
UNIVERSITY OF CALIFORNIA

EARTH SCIENCES DIVISION

Submitted to Water Resources Research

On Thermohydrological Conditions near High-level Nuclear Wastes Emplaced in Partially Saturated Fractured Tuff

Part 1. Simulation Studies with Explicit Consideration of Fracture Effects

K. Pruess, J.S.Y. Wang, and Y.W. Tsang

October 1989

Prepared for the U.S. Department of Energy under Contract Number DE-AC03-76SF00098.

DISCLAIMER

LBL-24563

On Thermohydrological Conditions near High-level Nuclear Wastes Emplaced in Partially Saturated Fractured Tuff

Part 1. Simulation Studies with Explicit Consideration of Fracture Effects

K. Pruess, J. S. Y. Wang, and Y. W. Tsang

Earth Sciences Division
Lawrence Berkeley Laboratory
1 Cyclotron Road
Berkeley, California 94720

October 1989

This work was supported by the Yucca Mountain Project, Sandia National Laboratories, and by the Director, Office of Energy Research, Office of Basic Energy Sciences, Engineering and Geosciences Division, of the U.S. Department of Energy under Contract No. DE-AC03-76SF00098.

LBL-24563

SAND 86-7015J

On Thermohydrological Conditions near High-level Nuclear Wastes Emplaced in Partially Saturated Fractured Tuff

Part 1. Simulation Studies with Explicit Consideration of Fracture Effects

K. Pruess, J.S.Y. Wang, and Y.W. Tsang

Earth Sciences Division, Lawrence Berkeley Laboratory
University of California, Berkeley, California 94720

Abstract

We have performed modeling studies on the simultaneous transport of heat, liquid water, vapor, and air in partially saturated, fractured porous rock. Formation parameters were chosen as representative of the potential nuclear waste repository site in the Topopah Spring Unit of the Yucca Mountain tuffs. The presence of fractures makes the transport problem very complex, both in terms of flow geometry and physics. The numerical simulator used for our flow calculations takes into account most of the physical effects believed to be important in multiphase fluid and heat flow. It has provisions for handling the extreme nonlinearities that arise in phase transitions, component disappearances, and capillary discontinuities at fracture faces.

We model a region around an infinite linear string of nuclear waste canisters, taking into account both the discrete fractures and the porous matrix. Thermohydrologic conditions in the vicinity of the waste packages are found to depend strongly on relative permeability and capillary pressure characteristics of the fractures, which are unknown at the present time. If liquid held on the rough walls of drained fractures is assumed to be mobile, strong heat pipe effects are predicted. Under these conditions the host rock will remain in two-phase conditions right up to the emplacement hole, and formation temperatures will peak near 100°C. If it is assumed that liquid cannot move along drained fractures, the region surrounding the waste packages is predicted to dry up, and formation temperatures will rise beyond 200°C. A substantial fraction of waste heat can be removed if emplacement holes are left open and ventilated, as opposed to backfilled and sealed emplacement conditions. Comparing our model predictions with observations from in situ heater experiments reported by Zimmerman and coworkers, some intriguing similarities are noted. However, for a quantitative evaluation, additional carefully controlled laboratory and field experiments will be needed.

1. Introduction

The U.S. Department of Energy is currently performing detailed studies at Yucca Mountain to determine its suitability as a host for a geologic repository for high-level nuclear wastes. The thick tuff formations at Yucca Mountain, Nevada, are located above the water table in partially saturated rock. The problems of site characterization and evaluation and repository performance assessment pose themselves rather differently in this setting as compared to fully saturated formations below the water table.

For nuclear waste disposal below the water table, desirable conditions include (1) very low permeability of the intact rock, (2) sparseness and lack of connectivity of fractures, and (3) preservation of the mechanical integrity of the rock during repository construction and during the period of thermally induced stress. The unsaturated tuffs at Yucca Mountain do have very low matrix permeability, of the order of 10^{-18} m^2 (1 microdarcy; Peters et al., 1984; Reda, 1985; Tien et al., 1985), but their waste isolation capability may not depend upon the sparsity of natural or thermally induced fractures. In fact, at the potential repository horizon in the Topopah Spring unit, fracturing is intense with fracture spacing of the order of 0.3 m (Scott et al., 1982; Montazer and Wilson, 1984). The fractures are believed to be generally well connected, with average permeability estimated in the range of 10^{-16} to 10^{-11} m^2 (0.1 millidarcy to 10 darcy; Winograd and Thordarson, 1975; Thordarson, 1983; Peters and Gauthier, 1984; Peters et al., 1986). The waste isolation capability of this kind of formation is brought about by hydrologic mechanisms which under partially saturated conditions tend to restrict water flow to the very tight rock matrix (Wang and Narasimhan, 1985). With few exceptions (notably C-14), the contaminants which could be released from high-level nuclear waste packages can only migrate when dissolved in the liquid phase, which under "normal" (ambient) conditions is held in the rock matrix by extremely strong capillary and adsorptive forces. Even under rather unlikely conditions of prevalent fracture flow, contaminant migration may be very slow because of diffusion into the matrix pores (Neretnieks and Rasmuson,

1984).

For waste package and repository design and performance assessment, reliable methods are needed for predicting future hydrologic and chemical conditions at the waste packages and in the surrounding medium. Besides laboratory and field experimentation, an important means by which this can be accomplished is mathematical modeling (computer simulation).

Several workers have performed modeling studies of effects from the thermal loading of high-level nuclear wastes. Mondy et al. (1983) simulated fluid and heat flow for approximate two-dimensional representations of alternative emplacement geometries with and without ventilation of emplacement drifts. The host rock was modeled as an unfractured porous medium, and no allowance was made for vaporization or vapor transport (two-phase) effects. Because of the relatively coarse space discretization, it was not possible to resolve the detailed temperature distribution near the waste packages. The maximum rock temperature predicted from the model was 110°C.

A thermal analysis for waste package emplacement in vertical boreholes was presented by St. John (1985). He modeled heat conduction (no fluid flow) in realistic two- and three-dimensional emplacement geometries. Maximum host rock temperatures were found to be near 250°C.

Sensitivity studies on thermohydrological conditions near an infinite linear string of waste packages were reported by Pruess and Wang (1984). They modeled fluid and heat flow, including phase change effects, in one-dimensional cylindrical geometry. The host formation was represented as a porous medium, and formation parameters were varied to examine the conditions under which the region surrounding the waste packages would dry up or remain wet. Strong two-phase vapor-liquid counterflow effects known as "heat pipe" (Ogniewicz and Tien, 1979; Udell, 1985) were observed in some cases. Extending the one-dimensional linear analysis of Udell (1985), Doughty and Pruess (1987) recently developed a semianalytical solution for heat pipe effects near high-level nuclear wastes emplaced in partially saturated media.

The coupling with mechanical deformations of the rock has been investigated in field experiments by Zimmerman and coworkers (Zimmerman, 1983; Zimmerman et al., 1985; Zimmerman and Blanford, 1986). Studies of chemical composition and transport effects have been presented recently by a number of authors (see e.g., Travis et al., 1984; Braithwaite and Nimick, 1984; Nielsen et al., 1986; Travis and Nuttall, 1987).

In this paper, we focus exclusively on thermal and hydrologic effects. We present and apply numerical simulation techniques for describing the thermal and hydrologic processes and conditions following emplacement of heat-generating waste packages in a partially saturated fractured-porous medium. More specifically, our objectives are to demonstrate a capability for modeling non-isothermal flow of water and air with phase change in a fractured medium and to obtain initial insight into expected thermohydrological conditions near the waste packages. In our simulation studies, we attempt to resolve in detail the complex fluid and heat transfer processes near the interface between rock matrix and fractures and to identify the controls on the behavior of the flow system. Such detailed modeling is feasible only for limited space- and time-scales. In a companion paper (Part 2, this issue), we present an "effective continuum" approach, based on insights gained from the detailed studies presented in this paper. This approach can provide a substantial simplification of the flow problem, so that calculations for large space- and time-scales become feasible. Portions of this work have been published previously in abbreviated form (Pruess et al., 1985).

2. Coupled Fluid and Heat Flow

The tuff formations at Yucca Mountain consist of thick layers (up to several hundred meters) of alternating welded and nonwelded units with large contrast in degree of fracturing and rock matrix permeability and porosity (Montazer and Wilson, 1984; Peters et al., 1984; Tien et al., 1985). The potential repository horizon is located in the Topopah Spring welded unit at approximately 350 m beneath the ground surface and 225 m above the water table (Tsang and Pruess, 1987). This unit is highly fractured (approximately 40 fractures per cubic meter; Scott et al., 1982). It has been estimated that 65% ± 19% of

the pore volume contains water, held in the porous matrix by capillary suction (Montazer and Wilson, 1984). It is assumed that the remaining voids contain air and a small amount of water vapor at ambient pressures and temperatures (P = 1 bar, T = 26°C).

Emplacement of high-level nuclear wastes in this environment will give rise to strong two-phase flow effects. As heat released from the waste packages is transferred to the host rock, temperatures near the waste packages will approach or exceed the boiling point of water (approximately 100°C at ambient pressures). Vaporization of formation water will then take place, with associated increases in vapor partial pressure and overall gas phase pressure. This will give rise to forced convection of the gas phase with redistribution of water accompanied by large latent heat effects. The phase transformation and gas phase flow effects will perturb the original saturation distribution in the rock matrix, thereby setting up capillary pressure gradients and liquid phase flow.

To describe the hydrologic and thermal conditions near the waste packages, it is necessary to employ a multiphase approach to fluid and heat flow, that fully accounts for the movement of gaseous and liquid phases, their transport of latent and sensible heat, and phase transitions between liquid and vapor. The gas phase will, in general, consist of a mixture of water and air, and both these components must be kept track of individually.

Recently developed modeling capabilities for strongly heat-driven multi-phase flow borrow from techniques used in the simulation of geothermal reservoirs and enhanced oil recovery operations (Pruess and Wang, 1987). Available numerical simulators for variably saturated nonisothermal flow employ generally similar mathematical and numerical methods (Travis, 1983; Eaton, 1983; Eaton et al., 1983; Pruess and Wang, 1984; Hadley, 1985; Bixler, 1985; Travis et al., 1985; Pollock, 1986; Pruess, 1987). In the present work, we use the TOUGH code, which accounts for all processes indicated with a dot in Table 1 (Pruess, 1987). The governing equations solved by TOUGH, summarized in the appendix, are highly nonlinear because of order-of-magnitude changes in parameters during phase transitions and because of nonlinear material properties (chiefly relative permeability and capillary pressure functions). Furthermore, the mass- and energy-balance equations are strongly coupled. Because of these features of the equation system, TOUGH performs a completely simultaneous solution of the discretized mass- and energy-balance

equations, taking all coupling terms into account. Space discretization is made with the integral finite difference (IFD) method (Narasimhan and Witherspoon, 1976). This method avoids any reference to a global system of coordinates, so that one-, two-, and three-dimensional flow systems with regular or irregular geometry can be treated on the same footing. Furthermore, this method is applicable to porous as well as fractured-porous media (Narasimhan, 1982; Pruess and Narasimhan, 1985). Time is discretized fully implicitly as a first-order finite difference to obtain the numerical stability needed for an efficient calculation of flow in fractured media with extremely small fracture volumes. The coupled nonlinear equations are solved by means of Newton-Raphson iteration. Time steps are increased or decreased automatically during execution, as required to achieve convergence of the Newton-Raphson process within a "reasonably" small number of iterations (typically 3 to 6). The linear equations arising at each iteration step are solved by LU-decomposition and back substitution, using sparse storage techniques (Duff, 1977). The numerical accuracy of TOUGH has been verified by solving a number of geothermal reservoir and unsaturated fluid and heat flow problems for which (semi-) analytical or numerical solutions are available (Pruess, 1987).

3. Modeling Approach

A quantitative description of fluid and heat flow near high-level waste packages emplaced in partially-saturated fractured rock must deal with three distinct difficulties: (1) A variety of complex physical and chemical processes are taking place (see Table 1); (2) several parameters of major significance for the hydrologic processes are poorly known at the present time (this is especially true for permeability, porosity, and characteristic curves of the fractures); and (3) the flow geometry near the waste packages is three-dimensional and involves complicated detail on a small scale (fracture spacing of the order of 0.3 m; fracture apertures of the order of 10-100 μm; Scott et al., 1982; Peters et al., 1984). In the present work, we have followed a two-track approach. We begin by studying fluid and heat flow processes near high-level waste packages on a small spatial scale, where the processes operating on the level of individual fractures and

matrix/fracture interfaces can be resolved in detail. To accomplish this, it is necessary to idealize fracture and waste emplacement geometry. Specifically, we consider an infinite linear string of waste packages intersected by one set of plane, parallel, infinite fractures at a right angle (Figure 1). Further neglecting gravity effects, only one symmetry element then needs to be modeled, as indicated by dashed lines in Figure 1. This results in a two-dimensional idealized model, the geometric simplicity of which makes it possible to obtain the desired detailed description of fluid and heat flow processes.

In the simulations, the fractures are modeled as very small spatial domains with large permeability (see Tables 2 and 3). On the basis of the results obtained for the detailed model, we then develop an approximation in which the complexity of dual-porosity behavior is replaced by a single "effective continuum" description (Part 2, this issue). Such an approach will be needed for practical applications where it is neither possible nor desirable to account for detail on the level of individual fractures.

4. Problem Specifications

As mentioned above, some of the important hydrologic parameters applicable to the Topopah Spring unit are not well known at present. Most of the parameters used in the present study were provided by Sandia National Laboratories (Hayden et al., 1983); they represent the best estimates available at the beginning of this work. A number of different cases were studied to explore how thermohydrologic behavior changes when some of the less well known parameters are modified. Even as improved parameter estimates became available in the course of this work, we continued to use the original data set so that results for the different cases would be comparable.

A summary of the formation parameters is given in Table 2. Data on characteristic curves are available only for the rock matrix. To make an estimation for characteristic curves of the fractures, we proceeded as follows. Upon close examination of the measured suction curve for the tuff matrix (Hayden et al., 1983; see Figure 2), it is apparent that the very strong suction pressures such as −2000 bars at low liquid saturation in the matrix ($S_{l,m}$ = 2%) cannot represent effects of capillary pressure related to curvature of

the matrix pores. Indeed, the capillary radius corresponding to $P_{suc} = -2000$ bars is $r_{cap} = -2\sigma/P_{suc} = 7.3 \times 10^{-10}$ m (where $\sigma = 0.072$ N/m is the surface tension of water at ambient temperature), or approximately twice the diameter of the water molecule! In this range of low liquid saturation, the suction curve in fact represents the effects of liquid phase adsorption on the solid surface of the rock (Philip, 1978; Herkelrath and O'Neal, 1985). The transition from capillary mechanism to adsorption mechanism has been studied in concrete slabs (Huang et al., 1979). Since the adsorption mechanism depends only on physical and chemical properties of the solid, liquid, and gaseous phases involved, but not on the curvature of the pore spaces, we expect that the phase adsorption effects observed for the tuff matrix will also be present on fracture surfaces. The ambient suction $P_{suc} = -10.93$ bars corresponds to an initial liquid saturation $S_{l,m} = 80\%$ in the matrix. Thus, liquid can be held by capillary force only in fractures with aperture $\delta < -2\sigma/P_{suc} = 13.2 \times 10^{-8}$ m. Therefore, the bulk of the fractures will be drained, and liquid can be present only on the fracture surfaces held either in surface roughness and asperities, or as a thin adsorbed film of a few molecular layers. We suggest that the very strong suction pressures at low liquid saturation for the matrix (as shown in Figure 2) are also encountered when the fractures are desaturated, except that most of this pressure range corresponds to a small (at present undetermined) interval of low liquid saturations in the fractures.

The thin film of liquid present on the walls of drained fractures presumably has low mobility. Specifically, we assume an immobile saturation $S_{lr,f}$ such that liquid relative permeability in the fractures $k_{rl,f}(S_{l,f}) = 0$ for $S_{l,f} \leq S_{lr,f}$. For $S_{l,f} > S_{lr,f}$, the liquid phase fracture relative permeability is assumed to be a linear function of liquid saturation with $k_{rl,f} = 1$ at $S_{l,f} = 1$ (Romm, 1972). Gas relative permeability is assumed equal to gas saturation, $k_{rg,f} = S_{g,f}$, so that $k_{rl,f} + k_{rg,f} = 1$, as suggested in the geothermal literature (Pruess et al., 1983). For definiteness and convenience, we assume an immobile liquid saturation of $S_{lr,f} = 1\%$; however, neither this particular value nor the assumption of vanishing liquid relative permeability for $S_{l,f} < S_{lr,f}$ are essential for our numerical experiments.

Since quantitative information on the suction pressures for fractures at low saturations is not presently available, we consider two cases which are intended to illustrate alternative possible system behavior. These cases differ with respect to mobility of liquid in the fractures at the initial (pre-emplacement) suction pressure. In the first case, we assume for simplicity that $P_{suc,f}$ varies linearly between 0 and the limiting value of −5000 bars used in the matrix for the saturation interval $0.0099 > S_{l,f} > 0$. Before waste package emplacement, matrix and fractures will be in capillary equilibrium. At the assumed initial matrix saturation of $S_{l,m} = 80\%$ we have $P_{suc} = -10.93$ bars. This value is attained in the fractures at a liquid saturation of $S_{l,f} = 0.9878\%$, which we use as initial condition in our problem (Fig. 3). Note that this saturation is just barely below the assumed irreducible saturation in the fractures of $S_{lr,f} = 1.0\%$, so that initially, liquid is immobile in the fractures (see Figure 3).

In the second case, we assume that the linear variation of P_{suc} with $S_{l,f}$ occurs over a larger range, namely, $0.05 > S_{l,f} > 9.6 \times 10^{-4}$, so that capillary equilibrium between matrix and fractures is attained at a saturation $S_{l,f} > S_{lr,f}$, and liquid is (slightly) mobile in the fractures at initial conditions. One of the most numerically difficult aspects of the first case, where P_{suc} varied from 0 to −5000 bars in the range of $0.0099 > S_{l,f} > 0$, is the extremely large slope $dP_{suc}/dS_{l,f} = 5 \times 10^5$ bars. To facilitate calculations in the second case, we arbitrarily diminish maximum strength of suction pressure to −50 bars, resulting in a more modest slope of $dP_{suc}/dS_{l,f} = 10^3$ bars. As it turns out in the simulation, liquid saturation in the fractures never changes by more than $1.2 \times 10^{-3}\%$, so that only the slope $dP_{suc}/dS_{l,f}$ is of significance here, whereas the maximum absolute strength of P_{suc} is irrelevant. The same linear relative permeability functions as in Case 1 were used, except that we take $S_{lr,f} = 0$. Initial capillary equilibrium in Case 2 is attained at $S_{l,f} = 3.928\%$, at which saturation liquid relative permeability is $k_{l,f} = 3.93 \times 10^{-2}$.

Fluid and heat flow calculations with explicit representation of fractures require much numerical work because time step sizes are limited by the small volume elements representing fractures, and because the interporosity flow between rock matrix and fractures adds an extra dimension to the flow problem. It is not clear exactly how small fracture apertures must be specified to obtain a realistic representation of fluid and heat flow

effects. It has been suggested that fracture apertures in the Topopah Spring unit may be in the range of a few to several hundred microns (Peters et al., 1984; Zimmerman and Blanford, 1986). The "cubic law" (Witherspoon et al., 1980) can be used to estimate the equivalent parallel-plate aperture of individual fractures, δ, from data on fracture spacing D and the average permeability $\bar{k}_f$, of the fracture network:

$$\delta = (12D\bar{k}_f)^{1/3} \tag{1}$$

Using the data for D and $\bar{k}_f$ given in Table 2, we obtain δ = 64.15 microns. The corresponding equivalent continuum porosity of the fractures is then 0.029%. However, recent hydraulic and tracer tests have established that fracture apertures, in the sense of void volume per unit surface area, can be several orders of magnitude larger than would be deduced from a parallel-plate model (Abelin et al., 1987). This has been attributed to effects from surface roughness and tortuosity (Tsang and Tsang, 1987). It appears that for "real" (rough-walled) fractures, permeability and aperture should be regarded as essentially independent parameters, permeability being controlled by the flow constrictions, while porosity is controlled by the largest voids. These considerations suggest that fracture apertures in the Topopah Spring unit may be considerably larger than the parallel-plate value of 64.15×10^{-6} m.

From a numerical viewpoint, it is desirable to simplify the description of fractures. This can be done by using a larger aperture than estimated from a parallel-plate model, because it is the small volume elements in the fractures which control and limit time step size. Furthermore, it would be advantageous to include wall rock to a certain depth into the fracture elements, as this will increase their thermal mass and the attainable time steps. We have performed calculations for a parallel-plate as well as for a "coarse" description of the fractures (see Table 2). In the "coarse" description, a "fracture" is specified as a domain of 2 mm width, of which 20% corresponds to void space while the remainder contains rock grains. Average fracture porosity in the continuum sense is then 0.182%, which is consistent with the range of observed fracture porosities in a wide variety of geologic media (Weber and Bakker, 1981).

The calculations were carried out with two different two-dimensional r-z grids, with parameters given in Table 3. The "coarse" grid was used in conjunction with the coarse fracture specifications, while the fine grid was used for the parallel-plate fractures. Thus, a comparison between the two cases will allow evaluation of differences in fluid and heat flow behavior from the different parametrization of the fractures, and it will provide insight into numerical truncation errors associated with spatial discretization. In addition, we have performed simulations with different time step controls to examine time truncation errors.

We have simulated "open-hole" as well as backfilled conditions. In the open-hole calculations, we assume that the space between waste packages and host rock is void and is connected via essentially infinite permeability to an infinite air reservoir at a pressure of 1 bar, which represents the mined openings and the connection to the atmosphere (ventilation). For the backfilled conditions the space around the waste is assumed to contain material with properties identical to the rock matrix. The waste package itself is modeled as impermeable material with time-varying rate of heat generation corresponding to 10-year-old spent fuel (Hayden et al., 1983). At the time of waste emplacement, thermal power per waste package is 3.051 kW. Heat flux is assumed to be uniform over the entire surface of the waste package (Neuman boundary condition). For convenience, all results for extensive quantities such as fluid and heat flow rates will be reported on a "per-waste-package basis." The calculations were performed in part on a Control Data CDC-7600 computer, and in part on the Cray XMP at the National Magnetic Fusion Energy Computing Center.

5. Simulated Flow Behavior

We shall here describe the simulated response of the fractured-porous medium to waste emplacement in general terms, as shown schematically in Figure 4. Subsequently the quantitative results will be discussed.

Emplacement of the waste packages causes temperatures to rise in both rock matrix and fractures. Initially, this causes evaporation of a modest amount of liquid water, as the

partial pressure of vapor increases according to the saturated vapor pressure curve, $P_v = P_{sat}(T)$. Boiling becomes vigorous as the formation temperatures approach 100°C. Most vapor generated in the rock matrix flows towards the fractures. In addition, liquid flows from the interior of the rock matrix towards the fractures, driven by gradients in (overall) pressure and capillary pressure; the liquid vaporizes as it encounters a (small) pressure drop upon entering the fractures. Subsequent system behavior depends upon whether the waste package hole is open or backfilled. The latter condition is somewhat simpler and will be discussed first.

The vapor generated in the fractures flows outward, away from the heat source, and soon condenses as it encounters cooler rock. In Case 1, where liquid is initially immobile in the fractures, the condensate re-enters the matrix under capillary suction. Subsequently, most of the liquid migrates by capillary force through the matrix down the saturation profile towards the boiling region near the waste package, while a smaller amount flows outward from the condensation zone. Because of the low matrix permeability, radial outflow of vapor in the fractures exceeds radial inflow of liquid in the matrix, so that the rock near the waste package becomes desaturated (dries up). As far as heat transfer is concerned, three distinct regions develop (see Figure 5). In the dried region near the waste package, heat flow occurs by conduction, with negligibly small contributions from gas flow in response to changing temperatures. Beyond the dried zone is a region with substantial heat transfer contributions from vapor-liquid counterflow. This mechanism, usually referred to as "heat pipe" (Eastman, 1968), in effect enhances the thermal conductivity of the medium, so that substantial heat fluxes can be transmitted over regions with small temperature gradients. In the present case, the heat pipe is of a transient nature because outflow of vapor exceeds inflow of liquid. Therefore, with time, the entire spatial pattern of vaporization in the matrix, vapor discharge into fractures, condensation at fracture walls, and subsequent liquid backflow in the matrix toward the heat source slowly migrates radially outward, away from the waste packages. Beyond the heat pipe region is another conduction zone, in which fluid flow contributions to heat transfer are negligibly small. Even though liquid had been just barely immobile in the fractures initially, it remained immobile at all times. The very slight saturation buildup

of $\Delta S_{l,f} > 0.0122\%$ that would be required to achieve liquid mobility in the fractures is never accomplished because capillary suction in the matrix is sufficiently strong to draw liquid out of the fractures at the same rate as it condenses.

Behavior of the condensed liquid is entirely different in Case 2, where liquid has a finite mobility in the fractures. The slight saturation changes in the fractures as a consequence of vaporization near the waste packages and condensation at some distance from them induce a suction gradient and associated liquid flux in the fractures. The extremely large fracture permeability gives rise to rapid movement of water away from the condensation zone, both radially inward and outward. In this way, the condensate is rapidly distributed over the fracture faces, with little water entering the matrix near the condensation front. Backflow of liquid towards the boiling region near the canisters is facilitated by the high-permeability pathway in the fractures. With time, a balanced vapor-liquid counterflow is established, which stabilizes the saturation profile near the canisters, and prevents the drying process from going very far. A stable heat pipe develops that extends all the way to the waste package hole, so that the inner conduction zone shown in Figure 5 is absent in this case. The gas phase "overpressure" needed to drive the heat pipe is small because of large fracture permeability. Gas phase pressure always remains close to 1 bar, so that the temperatures in the fractures remain near or below 100°C. Because of the small fracture spacing, flow paths for matrix-fracture flow are short (< 11 cm), and temperature and pressure conditions remain close to (T,P) = (100°C, 1 bar) even in the rock matrix. This is in contrast to Case 1, where temperatures rise to much higher values. These results suggest that the issue of liquid mobility on the faces of drained fractures warrants a thorough experimental investigation since it could have dramatic impacts on design parameters for waste packages.

For open-hole conditions, system behavior is basically similar to the cases discussed above, with one important difference. Prior to repository closure, the open hole is connected via practically infinite permeability to the atmosphere and acts as a pressure sink, with P = 1 bar. Therefore, a portion of the vapor generated in the fractures discharges into the waste package hole and is then removed from the system by ventilation. Besides affecting ventilation requirements, this vapor discharge also diminishes the net rate at

which heat enters the host rock. For the case with mobile liquid in the fractures, most vaporization occurs in the fractures in immediate proximity to the waste package hole. Therefore, vapor discharge into the hole takes place at a high rate, and a substantial fraction of total heat output is removed from the system by this vapor discharge. Rates of vapor discharge into the hole and associated heat flow are much smaller in the case with immobile liquid in the fractures because vapor is generated at a greater distance from the hole.

Under backfilled conditions, the processes of vaporization, vapor flow, and condensation merely give rise to redistribution of moisture within the host rock, whereas under open-hole conditions, some formation water is actually removed from the system. This sets up a capillary gradient that draws water from large distance toward the waste package hole. In effect, waste packages placed in open ventilated holes will suck moisture from the formation.

6. Space- and Time-Discretization Effects

Three simulation runs were performed to examine issues of fracture representation and space- and time-truncation errors (see Table 4). All these runs were done for open-hole conditions and Case 2 parameters (liquid mobile in fractures). Because calculations for parallel-plate fractures are very costly, the runs were carried out for only 11.1 days of physical time. This is sufficient to encounter boiling of formation water, which begins approximately 4.5 days after waste emplacement, and associated two-phase fluid flow and heat transfer effects. The "fine" and "coarse" fracture calculations (runs 1 and 2) can be viewed in two alternative ways. A first possible viewpoint is that those calculations examine the behavior of fracture sets which are physically different: the first set being parallel-plate, the second set being rather coarse and having considerable roughness and fill. Both sets have the same continuum permeability but differ somewhat in continuum porosity (see Table 2). According to this viewpoint the results of runs 1 and 2 then indicate the extent to which these two different fracture sets indeed behave differently for the particular thermohydrologic processes considered.

A second possible viewpoint is that both runs 1 and 2 treat essentially the same fracture set, but with different levels of spatial resolution. Apart from small effects of different storage in the slightly different equivalent continuum porosities, comparison of run 1 and 2 results then provides a measure of numerical space discretization effects. Both these viewpoints are important in establishing the role of fracture geometry and numerical discretization effects in the simulation of thermohydrologic flows in fractured porous media.

Time discretization errors were examined by performing the coarse grid calculations with two different time step controls (see Table 4). Run 2 uses the same time step limit as the fine grid calculation. In run 3, an automatic time step control was used, in which time step size was doubled whenever the Newton-Raphson process converged in no more than four iterations, and was reduced by a factor of four if convergence could not be achieved within nine iterations.

Results from these runs are given in Figures 6 and 7. Figure 6 shows the rate at which heat is removed from the system by vapor flow out of the emplacement hole. Discrepancies between the three calculations are generally small; they are largest during the rapid initial transient (4.5 to 7 days), and in this period, the deviations between runs 2 and 3 are much larger than those between runs 2 and 1, indicating that time truncation errors are far greater than space truncation errors. After 11 days, the maximum deviation is no more than 4.4%, with approximately equal contributions from space- and time-truncation errors. (Run 2 results are intermediate between those of runs 1 and 3.)

Figure 7 shows temperature and liquid flow rate patterns in the fracture after 11.1 days. Only run 1 temperatures are plotted because those for the other runs agree to within line thickness. Liquid flow rates agree to better than 5% throughout. Run 2 results are intermediate between those for runs 1 and 3 at small radius, indicating that space- and time-truncation errors contribute equally to the discrepancies at small radius. At larger radius the discrepancy between runs 2 and 3 is larger than that between runs 1 and 2, which indicates that the dominant contribution is made by time truncation errors. The deviations between the three runs are small compared to the present uncertainties in hydrologic data. We expect that with time, these deviations would further diminish as

transient changes slow down and flow conditions approach quasi-steady patterns. We conclude, therefore, that the coarse grid with "large" time steps gives entirely acceptable accuracy. Furthermore, the physical processes and conditions of fluid and heat flow of interest in this study can be adequately predicted on the basis of a "coarse" description of the fractures, even if in reality fracture characteristics were close to parallel-plate. The simulated results discussed in the next section were obtained using "coarse" fracture parameters (see Table 2).

7. Thermohydrologic Conditions near the Waste Packages

Simulated temperatures in the host rock at 3.5 cm from the wall of the emplacement hole are shown in Figure 8 for backfilled emplacement conditions. Fracture and rock matrix temperatures are indistinguishable on the temperature scale used in that figure. For comparison, we have also plotted predictions obtained from a calculation without any fracture effects (Pruess, Tsang, and Wang, 1985). In the case where liquid is assumed immobile in the fractures temperatures are 10°C to 20°C lower than for the unfractured case, indicating that thermal effects of the fractures are not large in this case. When liquid is assumed mobile, a stable heat pipe develops that extends all the way to the wall of the emplacement hole, so that temperatures remain near 100°C. Thus, the presence or absence of liquid mobility in drained fractures has a profound effect on the expected thermohydrologic environment of the waste packages.

When the emplacement hole is assumed open and ventilated, moisture and heat are removed from the system at significant rates. Figure 9 shows that after a brief initial transient, only approximately 30% of total waste heat is transferred to the host rock for the case with mobile liquid in the fractures. The remainder is removed from the system in the form of latent heat of vapor discharging into the emplacement hole. Vapor discharge stabilizes at approximately 7×10^{-4} kg/s per waste package. If it is assumed that air for ventilation is supplied at ambient temperature and 20% humidity, and removed with negligible temperature increase at 95% humidity, the ventilation requirement can be estimated at approximately 0.04 m^3/s per waste package. Removal of heat by means of vapor

discharge into the open emplacement hole occurs at a much smaller rate when liquid is assumed immobile in the fractures (Figure 10). Furthermore, because in this case the region surrounding the emplacement hole dries up (see Figure 11), the region of most intense boiling migrates away from the emplacement hole with time, leading to a rapid temporal decline of vapor discharge into the hole (Figure 10).

In spite of net removal of heat through the open hole, temperatures near the emplacement hole wall are slightly higher for open-hole emplacement than for backfilled conditions for the case of immobile liquid in the fractures (Figure 12). This counterintuitive effect is caused by the fact that for open-hole emplacement, the heat pipe region (visible in Figure 12 as the plateau in the temperature curve near 100°C) is significantly shorter, because vapor pressures and the driving force for the heat pipe (vapor pressure gradients) are smaller.

The difference in heat pipe conditions between open and backfilled emplacement conditions is much stronger in the case where liquid is mobile in the fractures (Figure 13). One year after emplacement, the heat pipe extends from the wall of the emplacement hole out to approximately 3 m for the backfilled hole, but only out to 0.5 m for the open hole. This difference occurs because, in the open-hole case, a substantial loss of formation water occurs out to considerable distance, as is evident from the water saturation profile (Fig. 13). Therefore, gradients of liquid saturation, hence capillary pressure, are much weaker than in the backfilled case. Figure 14 shows temperature profiles for open-hole conditions at 1 and 10 yr after waste emplacement, respectively, indicating a growing region of quasi-steady conductive heat flow (temperature plotting as a straight line versus radial distance on semilog paper). This figure also shows that a nearly steady flow of liquid toward the emplacement hole develops in the fractures out to a great distance.

It is of interest to consider in more detail the nature of the drying process when liquid is assumed immobile in the fractures. Figure 15 shows "drying trajectories" for open-hole emplacement, in which liquid saturations at a point near the fractures (at a distance of 2 mm) are plotted against liquid saturations deep inside the matrix (at a distance of 64 mm from the fractures). If drying of the rock matrix proceeded in a uniform manner, the points in Figure 15 would move along the main diagonal toward the origin.

It is evident that near the waste package, a rather marked saturation profile evolves in the rock matrix, with regions in proximity to the fractures drying much more rapidly than regions deep in the matrix. At increasing distance from the heat source, the drying process becomes more and more uniform. A similar observation can be made for pressures inside the rock matrix. Figure 16 shows transients of gas phase pressure at 64 mm from the nearest fracture, at varying distances from the heat source. It is evident that with increasing distance from the waste package, pressures in the rock matrix rise less rapidly and remain closer to pressures in the fractures. These observations support the notion of "approximate local equilibrium" in describing the larger-scale behavior of the flow system, as discussed in more detail in the companion paper (Part 2, this issue).

8. Discussion and Conclusions

Our modeling studies predict that emplacement of a strong heat source in partially saturated, fractured tuff will give rise to complex phenomena of coupled fluid and heat flow with important phase transformation effects. In a quantitative sense, our results should be considered preliminary and approximate because of substantial idealizations and approximations made in the calculations. We have considered a highly idealized flow geometry to be able to represent fracture effects operating on a millimeter scale. Gravity effects were neglected which is expected to be admissible due to the strength of capillary forces in the strong saturation gradients near the waste packages (Doughty and Pruess, 1987). We have neglected effects of binary diffusion of vapor and air, which is believed to be a good approximation for the relatively small space- and time-scales considered here, where fluid flow is dominated by advection effects. A more important effect is Knudsen diffusion, also known as "slip flow," which is likely to considerably enhance effective gas permeability in the tuff matrix due to the small pore sizes (Knudsen, 1909; Klinkenberg, 1941; Hadley, 1982; Reda, 1987). The matrix permeability used in our analysis (32 microdarcies) is one to two orders of magnitude larger than more recent estimates (Reda, 1985; Klavetter and Peters, 1986), so that in some average sense, Knudsen effects are accounted for.

It is of interest to compare our modeling predictions with observations made in field experiments by Zimmerman and coworkers (Zimmerman, 1983; Zimmerman et al., 1985; Zimmerman and Blanford, 1986; Zimmerman et al., 1986). Because of different flow geometries and parameters, such a comparison can be made only in a qualitative sense. In the experiments, electric heaters of 120 cm length and 10.2 cm diameter were emplaced either vertically or horizontally in welded and nonwelded tuffs in G-tunnel, Nevada Test Site. Heater units with smaller dimensions than anticipated for high-level nuclear waste packages were used to obtain a more rapid thermal response of the host rock. Thermal and hydrologic properties and conditions of the G-tunnel tuffs cover the range expected at the target repository horizon at Yucca Mountain (Zimmerman et al., 1984). Over heating periods of up to 35 days, thermal output was varied between 400 and 1200 W. System response was monitored by means of a neutron probe (for saturation measurements) and by means of thermocouples, which were placed on the heater surface, on the surface of the emplacement hole, and in satellite holes approximately 20 cm away from the emplacement hole. Measured temperatures reached near 400°C at the heater surface, almost 300°C on the surface of the emplacement hole, and 150°C in the satellite hole. Vapor condensation effects were directly observed in the neutron probe measurements, which showed increasing liquid saturation outside of the strongly heated region.

In their most recent paper, Zimmerman and Blanford (1986) reported finite-element modeling studies of the experiments. They considered radiative and conductive heat transfer across the 2.5 cm gap between heater and emplacement hole, and conductive heat transfer only (no fluid flow) in the host rock. Some effects from formation fluids were taken into account by means of saturation-dependent thermal conductivity and by using effective formation heat capacities which include latent heat effects from phase change near 100°C. They were able to obtain generally satisfactory matches to observed temperatures.

In one of the experiments in welded tuff, the presence of water at the bottom of the heater hole was observed directly with a water level indicator and indirectly from temperature readings that remained at 94°C, the boiling temperature at ambient pressures in G-tunnel, for 33 hr after the start of heating. In another experiment, hydrothermal

phenomena were observed that appeared to be related to known vertical fractures in the rock that intersected the horizontal emplacement hole. One thermocouple mounted on the rock surface beneath the heater reached a temperature of 95°C after 12 days of heating, and remained at that temperature for 17 days. Subsequently, it increased to over 200°C within a few days. Another thermocouple did not exceed 95°C until after 32 days of heating. The (intermittent) stabilization of temperatures at saturated values for ambient pressures provides clear evidence for the presence of two-phase conditions. There are two mechanisms by which two-phase conditions can be maintained, namely, migration of vapor toward the hole with condensation in cooler portions of it, or direct migration of liquid toward the hole (heat pipe), presumably along fractures. From the data presented by Zimmerman and Blanford (1986), it is not possible to demonstrate conclusively the presence or absence of either mechanism. However, the field observations suggest that some transient heat pipe process was taking place in the fractures, as observed in our numerical modeling studies.

In summary, the G-tunnel heater experiments have produced hydrothermal phenomena that show intriguing similarities to some of the processes observed in our numerical modeling. Further carefully controlled field and laboratory heater experiments are needed to better define the important physical phenomena. A primary objective of such experiments should be to determine the extent to which liquid water can flow along the walls of ''drained'' fractures since such flow may have strong effects on waste package environment and on overall performance of the waste isolation system.

If it is assumed that water held on the rough walls of drained fractures is mobile, our simulation studies indicate that the host rock near the emplacement holes will remain in two-phase condition (no drying-up), with maximum formation temperatures near 100°C. On the other hand, if liquid is assumed to be immobile in drained fractures the region surrounding the emplacement holes is predicted to dry up and reach temperatures of approximately 250°C.

Thus, our simulation studies predict that liquid flow in drained fractures will produce a very characteristic and easily discernible thermal signature. This may prove a convenient means of experimentally tackling the issue of liquid flow in drained fractures,

which may strongly impact on chemical transport and long-term repository system performance.

Acknowledgement

This work was supported by the Yucca Mountain Project, Sandia National Laboratories, and the U.S. Department of Energy, Office of Basic Energy Sciences, under Contract No. DE-AC03-76SF00098. The authors appreciate a critical review of the manuscript and the suggestion of improvements by C. Doughty, S. Benson, B. Langkopf, P. Kaplan and S. Passman. We also acknowledge technical editing by Sandia National Laboratories.

References

Abelin, H., Birgersson, L., Gidlund, J., Moreno, L., Neretnieks, I., and Tunbrant, S., Results from some tracer experiments in crystalline rocks in Sweden, in C. F. Tsang (ed.), Coupled Processes Associated with Nuclear Waste Repositories, Academic Press, Inc., New York, 1987.

Bixler, N. E., NORIA - A finite element computer program for analyzing water, vapor, air, and energy transport in porous media, Sandia National Laboratories, Report SAND84-2057, Albuquerque, NM, August 1985.

Braithwaite, J. W., and Nimick, F. B., Effect of host-rock dissolution and precipitation on permeability in a nuclear waste repository in tuff, Sandia National Laboratories, Report SAND84-0192, Albuquerque, NM, September 1984.

Doughty, C., and Pruess, K., A semi-analytical solution for heat pipe effects near high-level nuclear waste packages buried in partially saturated geologic media, Lawrence Berkeley Laboratory Report LBL-23023, Berkeley, CA, February 1987 (in press, Int. J. of Heat and Mass Transfer).

Duff, I. S., MA28 - A set of FORTRAN subroutines for sparse unsymmetric linear equations, AERE Harwell report R8730, July 1977.

Eastman, G. Y., The heat pipe, Scientific American, Vol. 218, No. 5, pp. 38-46, May 1968.

Eaton, R. R., A numerical method for computing flow through partially saturated porous media, paper presented at International Conference on Numerical Methods in Thermal Problems, Seattle, WA, August 1983.

Eaton, R. R., Gartling, D. K., and Larson, D. E., SAGUARO - A finite element computer program for partially saturated porous flow problems, Sandia National Laboratories, Report SAND82-2772, Albuquerque, NM, June 1983.

Edlefsen, N. E., and Anderson, A. B. C., Thermodynamics of soil moisture, Hilgardia, Vol. 15, No. 2, pp. 31-298, 1943.

Hadley, R. G., Theoretical treatment of evaporation front drying, Int. J. Heat Mass Transfer, Vol. 25, No. 10, pp. 1511-1522, 1982.

Hadley, R. G., PETROS - A program for calculating transport of heat, water, water vapor and air through a porous material, Sandia National Laboratories, Report SAND84-0878, Albuquerque, NM, May 1985.

Hayden, N. K., Peters, R. R. and Johnstone, J. K., memo to distribution, September 27, 1983.

Herkelrath, W. N., and O'Neal II, C. F., Water vapor adsorption in low-permeability rocks, International Association of Hydrogeologists (ed.), Memoires, Vol. XVII, Part 1, pp. 248-253, 1985.

Hirschfelder, J. O., Curtiss, C. F., and Bird, R. B., Molecular theory of gases and liquids, John Wiley and Sons, New York, 1954.

Huang, C. L. D., Siang, H. H., and Best, C. H., Heat and moisture transfer in concrete slabs, Int. J. Heat Mass Transfer, Vol. 22, pp. 251-266, 1979.

International Formulation Committee, A Formulation of thermodynamic properties of ordinary water substance, IFC Secretariat, Düsseldorf, Germany, 1967.

Klavetter, E., and Peters, R. R., Fluid flow in a fractured rock mass, Sandia National Laboratories, Report SAND85-0855, Albuquerque, NM, March 1986.

Klinkenberg, L. J., The permeability of porous media to liquids and gases, in: API Drilling and Production Practice, pp. 200-213, 1941.

Knudsen, M., Die Gesetze der Molekularstroemung und der inneren Reibungsstroemung der Gase durch Roehren, Annalen der Physik, Vol. 28, pp. 75-131, 1909.

Mondy, L. A., Wilson, R. K., and Bixler, N. E., Comparison of waste emplacement configurations for a nuclear waste repository in tuff. IV. Thermohydrological analysis. Sandia National Laboratories, Report SAND83-0757, Albuquerque, NM, August 1983.

Montazer, P., and Wilson, W. E., Conceptual hydrologic model of flow in the unsaturated zone, Yucca Mountain, Nevada, U.S. Geological Survey, Water Resources Investigations Report 84-4345, Lakewood, Colorado, 1984.

Narasimhan, T. N., Multi-dimensional numerical simulation of fluid flow in fractured porous media, Water Resources Research, Vol. 18, No. 4, pp. 1235-1247, August 1982.

Narasimhan, T. N., and P. A. Witherspoon, An integrated finite difference method for analyzing fluid flow in porous media, Water Resources Res., Vol. 12, No. 1, pp. 57-64, 1976.

Neretnieks, I., and Rasmuson, A., An approach to modeling radionuclide migration in a medium with strongly varying velocity and block sizes along the flow path, Water Resources Research, Vol. 20, No. 12, pp. 1823-1836, December 1984.

Nielsen, D. R., van Genuchten, M. Th., and Biggar, J. W., Water flow and solute transport

in the unsaturated zone, Water Resources Research, Vol. 22, No. 9, pp. 89S-108S, August 1986.

Ogniewicz, Y., and Tien, C. L., Porous heat pipe, in: Heat transfer, thermal control, and heat pipes, Walter B. Olstad, ed., Progress in Astronautics and Aeronautics, Vol. 70, Martin Summerfield, series ed., presented at AAIA Thermophysics Conference, Orlando, FL, June 1979.

Peters, R. R., and Gauthier, J. H., Results of TOSPAC calculations for Yucca Mountain, unpublished memo to F. W. Bingham, April 30, 1984.

Peters, R. R., Gauthier, J. H., and Dudley, A. L., The effect of percolation rate on water-travel time in deep, partially saturated zones, Sandia National Laboratories, Report SAND85-0854, Albuquerque, NM, February 1986.

Peters, R. R., Klavetter, E. A., Hall, I. J., Blair, S. C., Heller, P.R., and Gee, G. W., Fracture and matrix hydrologic characteristics of tuffaceous materials from Yucca Mountain, Nye County, Nevada, Sandia National Laboratories, Report SAND84-1471, Albuquerque, NM, December 1984.

Philip, J. R., Adsorption and capillary condensation on rough surfaces, J. of Phys. Chem., Vol. 82, No. 12, pp. 1379-1385, 1978.

Pollock, D. W., Simulation of fluid flow and energy transport processes associated with high-level radioactive waste disposal in unsaturated alluvium, Water Resources Research, Vol. 22, No. 5, pp. 765-775, 1986.

Pruess, K., TOUGH user's guide, Nuclear Regulatory Commission, Report NUREG/CR-4645, June 1987 (also Lawrence Berkeley Laboratory Report LBL-20700, Berkeley, CA, June 1987).

Pruess, K., Bodvarsson, G. S., and Stefansson, V., Analysis of production data from the Krafla geothermal field, Iceland, paper presented at Ninth Workshop on Geothermal Reservoir Engineering, Stanford University, Stanford, CA, December 1983.

Pruess, K., and Narasimhan, T. N., A practical method for modeling fluid and heat flow in fractured porous media, Society of Petroleum Engineers Journal, Vol. 25, No. 1, pp. 14-26, February 1985.

Pruess, K., Tsang, Y. W., and Wang, J. S. Y., Modeling of strongly heat driven flow in partially saturated fractured porous media, International Association of Hydrogeologists (ed.), Memoires, Vol. XVII, pp. 486-497, 1985.

Pruess, K., and Wang, J.S.Y., TOUGH - A numerical model for nonisothermal unsaturated flow to study waste canister heating effects, in: G.L. McVay (ed.), Mat. Res. Soc. Symp. Proc., Vol. 26, Scientific Basis for Nuclear Waste Management, pp. 1031-1038, North Holland, New York, 1984.

Pruess, K., and Wang, J.S.Y., Numerical modeling of isothermal and nonisothermal flow in unsaturated fractured rock - A review, in "Flow and Transport through Unsaturated Fractured Rock," D. Evans and T. Nicholson (editors), American Geophysical Union, Geophysical Monograph 42, pp. 11-21, 1987.

Reda, D. C., Liquid permeability measurements on densely welded tuff over the temperature range of 25°C to 90°C, Sandia National Laboratories, Report SAND85-2482, Albuquerque, NM, December 1985.

Reda, D. C., Slip-flow experiments in welded tuff: The Knudsen diffusion problem, in C. F. Tsang (ed.), Coupled Processes Associated with Nuclear Waste Repositories, Academic Press, Inc., New York, 1987.

Romm, E. S., Fluid flow in fractured rocks, Moscow, 1966 (translated by W. R. Blake, Bartlesville, OK, 1972).

Scott, R. B., Spengler, R. W., Diehl, S., Lappin, A. R., and Chornack, M. P., Geologic character of tuffs in the unsaturated zone at Yucca Mountain, Southern Nevada, in *Role of the Unsaturated Zone in Radioactive and Hazardous Waste Disposal,* pp. 289-335, edited by J. Mercer, P. S. Rao, and I. W. Marine, Ann Arbor Science Publisher, Ann Arbor, MI, 1982.

St. John, C. M., Thermal analysis of spent fuel disposal in vertical emplacement boreholes in a welded tuff repository, Sandia National Laboratories, Report SAND84-7207, Albuquerque, NM, November 1985.

Thordarson, W., Geohydrologic data and test results from Well J-13, Nevada Test Site, Nye County, Nevada, Water-Resources Investigations Report 83-4171, U.S. Geological Survey, Denver, CO, 1983.

Tien, P. L., Siegel, M. D., Updegraff, C. D., Wahi, K. K., and Guzowski, R. V., Repository site data report for unsaturated tuff, Yucca Mountain, Nevada, Nuclear Regulatory Commission, Report NUREG/CR-4110, November 1985.

Travis, B. J., WAFE: A model for two-phase multi-component mass and heat transport in porous media, unpublished draft report, Los Alamos National Laboratory, 1983.

Travis, B. J., Hodson, S. W., Nuttall, H. E., Cook, T. L., and Rundberg, R. S., Numerical simulation of flow and transport in fractured tuff, Mat. Res. Soc. Symp. Proc., Vol. 26, pp. 1039-1047, Elsevier, New York, 1984.

Travis, B. J., Davis, A. H., Kunkle, T. D. and Deupree, R. G., KRAK - A computer

program for two-phase, two-component porous flow and fracture propagation, Los Alamos National Laboratory report LA-9703 (rev.), April 1985.

Travis, B. J. and Nuttall, H. E., Two-dimensional numerical simulation of geochemical transport in Yucca Mountain, Los Alamos National Laboratory report LA-10532-MS, December 1987.

Tsang, Y. W., and Pruess, K., A study of thermally induced convection near a high-level nuclear waste repository in partially saturated fractured tuff, Water Resources Res., Vol. 23, No. 10, pp. 1958-1966, October 1987.

Tsang, Y. W., and Tsang, C. F., Channel model of flow through fractured media, Water Resources Res., Vol. 23, No. 3, pp. 467-479, March 1987.

Udell, K. S., Heat transfer in porous media considering phase change and capillarity - The heat pipe effect, Int. J. Heat and Mass Transfer, Vol. 28, No. 2, pp. 485-495, 1985.

van Genuchten, M.Th., A closed-form equation for predicting the hydraulic conductivity of unsaturated soils, Soil Sci. Soc. Am. J., Vol. 44, pp. 892-898, 1980.

Wang, J. S. Y., and Narasimhan, T. N., Hydrologic mechanisms governing fluid flow in a partially saturated, fractured, porous medium, Water Resources Research, Vol. 21, No. 12, pp. 1861-1874, December 1985.

Weber, K. J., and Bakker, M., Fracture and vuggy porosity, paper SPE-10332, presented at the 56th Annual Fall Technical Conference and Exhibition of the SPE, San Antonio, TX, October 1981.

Winograd, I. J. and Thordarson, W., Hydrogeologic and hydrochemical framework, South Central Great Basin, Nevada-California, with special reference to the Nevada Test Site, U.S. Geological Survey Professional Paper 712-C, pp. C1-126, 1975.

Witherspoon, P. A., Wang, J. S. Y., Iwai, K., and Gale, J. E., Validity of cubic law for fluid flow in a deformable rock fracture, Water Resources Research, Vol. 16, No. 6, pp. 1016-1024, 1980.

Zimmerman, R. M., First phase of small diameter heater experiments in tuff, paper presented at 24th U.S. Symposium on Rock Mechanics, Texas A & M University, College Station, TX, June 1983.

Zimmerman, R. M., and Blanford, M. L., Expected thermal and hydrothermal environments for waste emplacement holes based on G-tunnel heater experiments, Proceedings, 27th U.S. Symposium on Rock Mechanics, pp. 874-882, U. of Alabama, June 1986.

Zimmerman, R. M., Blanford, M. L., Holland, J. F., Schuch, R. L., and Barrett, W. H., Final report G-tunnel small-diameter heater experiments, Sandia National Laboratories, Report SAND84-2621, Albuquerque, NM, December 1986.

Zimmerman, R. M., Nimick, F. B., and Board, M. B., Geoengineering characterization of welded tuffs from laboratory and field investigations, Proc., VIII Symposium on Scientific Basis for Nuclear Waste Management, Boston, MA, 1984.

Zimmerman, R. M., Wilson, M. L., Board, M. P., Hall, M. E., and Schuch, R. L., Thermal-cycle testing of the G-tunnel heated block, paper presented at 26th U.S. Symposium on Rock Mechanics, Rapid City, South Dakota, June 1985.

Appendix: Governing Equations of the TOUGH Simulator

TOUGH solves discretized versions of the following mass- and energy-balance equations

$$\frac{d}{dt}\int_{V_n} M^{(\kappa)} dV = \int_{\Gamma_n} \underset{\sim}{F}^{(\kappa)} \cdot \underset{\sim}{n} d\Gamma + \int_{V_n} q^{(\kappa)} dV \tag{1}$$

where κ = 1: water; κ = 2: air; κ = 3: heat. The term on the left hand side represents accumulation of mass (or heat), while the terms on the right hand side represent flow and sink/source terms, respectively.

The mass accumulation terms (κ = 1,2) are

$$M^{(\kappa)} = \phi \sum_{\beta=l,g} S_\beta \rho_\beta X_\beta^{(\kappa)} \tag{2}$$

where ϕ is porosity, S_β is saturation of phase β (= liquid, gas), ρ_β is density of phase β, and $X_\beta^{(\kappa)}$ is the mass fraction of component κ present in phase β. The heat accumulation term contains rock and fluid contributions

$$M^{(3)} = (1-\phi)\rho_R C_R T + \phi \sum_{\beta=l,g} S_\beta \rho_\beta u_\beta \tag{3}$$

where ρ_R is rock grain density, C_R is rock specific heat, T is temperature, and u_β is specific internal energy of phase β.

The mass flux terms contain a sum over phases

$$\underset{\sim}{F}^{(\kappa)} = \sum_{\beta=l,g} \underset{\sim}{F}_\beta^{(\kappa)} \tag{4}$$

where the flux in each phase is

$$\underset{\sim}{F}_\beta^{(\kappa)} = -k \frac{k_{r\beta}}{\mu_\beta} \rho_\beta X_\beta^{(\kappa)} (\nabla P_\beta - \rho_\beta \underset{\sim}{g}) - \delta_{\beta g} D_{va} \rho_\beta \nabla \left[X_\beta^{(\kappa)} \right] \tag{5}$$

Here k is absolute permeability, $k_{r\beta}$ is relative permeability of phase β, μ_β is

viscosity of phase β, $P_\beta = P + P_{cap,\beta}$ is the pressure of phase β (sum of a reference phase pressure and capillary pressure), and $\underset{\sim}{g}$ is gravitational acceleration. The last term in equation (5) contributes only for gas-phase flow and represents a binary diffusive flux, with D_{va} the diffusion coefficient for vapor in air.

Heat flux contains conductive and convective components

$$\underset{\sim}{F}^{(3)} = -K\nabla T + \sum_{\substack{\beta = l,g \\ \kappa = 1,2}} h_\beta^{(\kappa)} \underset{\sim}{F}_\beta^{(\kappa)} \tag{6}$$

Here K is heat conductivity of the rock-fluid mixture, and h_β is specific enthalpy of phase β. The sink/source term in Eq. (1) involves an integral over the volumetric source rate q^κ for component κ.

The transport equations given above need to be complemented with constitutive relationships, which express all parameters as functions of a set of primary thermodynamic variables. The thermophysical properties of water substance are accurately represented by the steam table equations, as given by the International Formulation Committee (1967). Because of the strong suction pressure encountered in desaturating tuff, vapor pressure lowering effects can be very large. These are represented by Kelvin's equation (Edlefsen and Anderson, 1943).

$$P_v(T,S_l) = P_{sat}(T) \cdot \exp\left[\frac{P_{cap}(S_l)}{\rho_l R(T + 273.15)}\right] \tag{7}$$

Air is approximated as an ideal gas, and additivity of partial pressures is assumed for air and vapor, $P_g = P_v + P_a$. The viscosity of air-vapor mixtures is computed from a formulation given by Hirschfelder et al., (1954), but using steam table values of vapor viscosity instead of approximations from kinetic gas theory. Henry's law is assumed for solubility of air in liquid water. Capillary pressures and relative permeabilities will usually depend on phase saturations, but more general relationships (e.g., temperature dependence) are possible.

Table 1. Physical Processes in Strongly Heat-Driven Flow in Partially Saturated Rocks*

1. Fluid Flow		2. Heat Flow
• pressure forces		• conduction
• viscous forces		• flow of latent and sensible heat
inertial forces		dispersion
• gravity		radiation
• interference between liquid and gas ("relative permeability")		viscous dissipation
		mechanical work
• dissolution of air in liquid		3. Vaporization and Condensation
• capillarity and adsorption		• temperature and pressure effects
• hysteresis	liquid	• capillarity and adsorption
differential heat of wetting		
chemical potential gradients		4. Changes in Rock Mass
• mixing of vapor and air		• thermal expansion
• vapor pressure lowering		• compression under stress
• binary diffusion	gas	thermal stress cracking
Knudsen diffusion		• mineral redistribution
thermodiffusion		

*Processes indicated with a dot have been studied with the TOUGH simulator.

Table 2. Formation Parameters

Matrix	
rock grain density	$\rho_R = 2550$ kg/m^3
rock specific heat	$C_R = 768.8$ J/kg°C
rock heat conductivity (dry)	$K = 1.6$ W/m°C
porosity	$\phi_m = 10.3\%$
permeability	$k_m = 32.6 \times 10^{-18}$ m^2
suction pressure	$P_{suc}(S_l) = -1.393\ (S_{EF}^{-1/\lambda} - 1)^{1-\lambda}$ MPa
relative permeability to liquid (van Genuchten, 1980)	$k_{rl}(S_l) = \sqrt{S_{EF}}\ [1 - (1 - S_{EF}^{1/\lambda})^{\lambda}]^2$
relative permeability to gas	$k_{rg}(S_l) = 1 - k_{rl}$ where $S_{EF} = (S_l - S_{lr})/(1 - S_{lr})$, $S_{lr} = 9.6 \times 10^{-4}$, $\lambda = 0.45$

Fractures (one vertical set)	"parallel-plate" fractures†	"coarse" fractures*
width	$\delta = 64.15 \times 10^{-6}$ m	2.0×10^{-3} m
porosity	$\phi_f = 100\%$	20%
spacing	$D = .22$ m	.22 m
average continuum permeability	$\bar{k}_f = 10^{-13}$ m^2	10^{-13} m^2
permeability per fracture	$k_f = \bar{k}_f \cdot D/\delta = 342.9 \times 10^{-12}$ m^2	11×10^{-12} m^2
equivalent continuum porosity	$\bar{\phi}_f = \phi_f\ \delta/D = 0.029\ \%$	0.182%

Initial Conditions	
temperature	$T = 26$°C
pressure	$P = 10^5$ Pa (≡ 1 bar)
liquid saturation in matrix	$S_{l,m} = 80\%$

† $k_f = \delta^2/12$

* No parallel-plate model implied for the fractures; k_f is less than the parallel plate permeability $(\phi_f\ \delta)^2/12 = 1.33 \times 10^{-8}$ m^2.

Table 3. Computational Grid for Explicit Fracture Calculations

The grid has a height of h = 0.11 m, corresponding to half the fracture spacing. It extends from the wall of the canister (r = 0.25 m) out to r = 300 m, at which distance boundary conditions of T = 26°C, P = 1 bar, S_l = 0.80 are maintained. Discretization in r-direction is made with a series of concentric cylinders with the following radii.

grid element	radius (m)	grid element	radius (m)	grid element	radius (m)
1	.2700	17	3.096	31	38.49
2	.3050	18	3.563	32	45.24
3	.3660	19	4.465	33	53.12
4	.4359	20	5.517	34	62.33
5	.5159	21	6.747	35	73.07
6	.6075	22	8.182	36	85.62
7	.7124	23	9.857	37	100.3
8	.8326	24	11.81	38	117.4
9	.9702	25	14.10	39	137.3
10	1.128	26	16.76	40	160.6
11	1.308	27	19.88	41	187.8
12	1.515	28	23.51	42	219.6
13	1.751	29	27.75	43	256.7
14	2.023	30	32.71	44	300.0
15	2.334				
16	2.689				

In z-direction, two different discretizations were used so that truncation errors could be examined. Layer A represents (half of) the fracture:

coarse discretization		fine discretization	
layer	thickness (m)	layer	thickness (m)
A	1×10^{-3}	A	32.08×10^{-6}
B	4×10^{-3}	B	67.92×10^{-6}
C	1.5×10^{-2}	C	0.2×10^{-3}
D	9.0×10^{-2}	D	0.7×10^{-3}
		E	2.0×10^{-3}
		F	7.0×10^{-3}
		G	2.0×10^{-2}
		H	3.0×10^{-2}
		I	5.0×10^{-2}

Table 4. Simulation Runs for Examining Discretization Errors

run	computational grid*	fracture description†	maximum time step (s)	number of time steps	CPU-time (minutes)
1	fine	parallel-plate	4×10^3	400	110.3
2	coarse	coarse	4×10^3	245	8.6
3	coarse	coarse	1×10^5	24	1.4

* see Table 3
† see Table 2

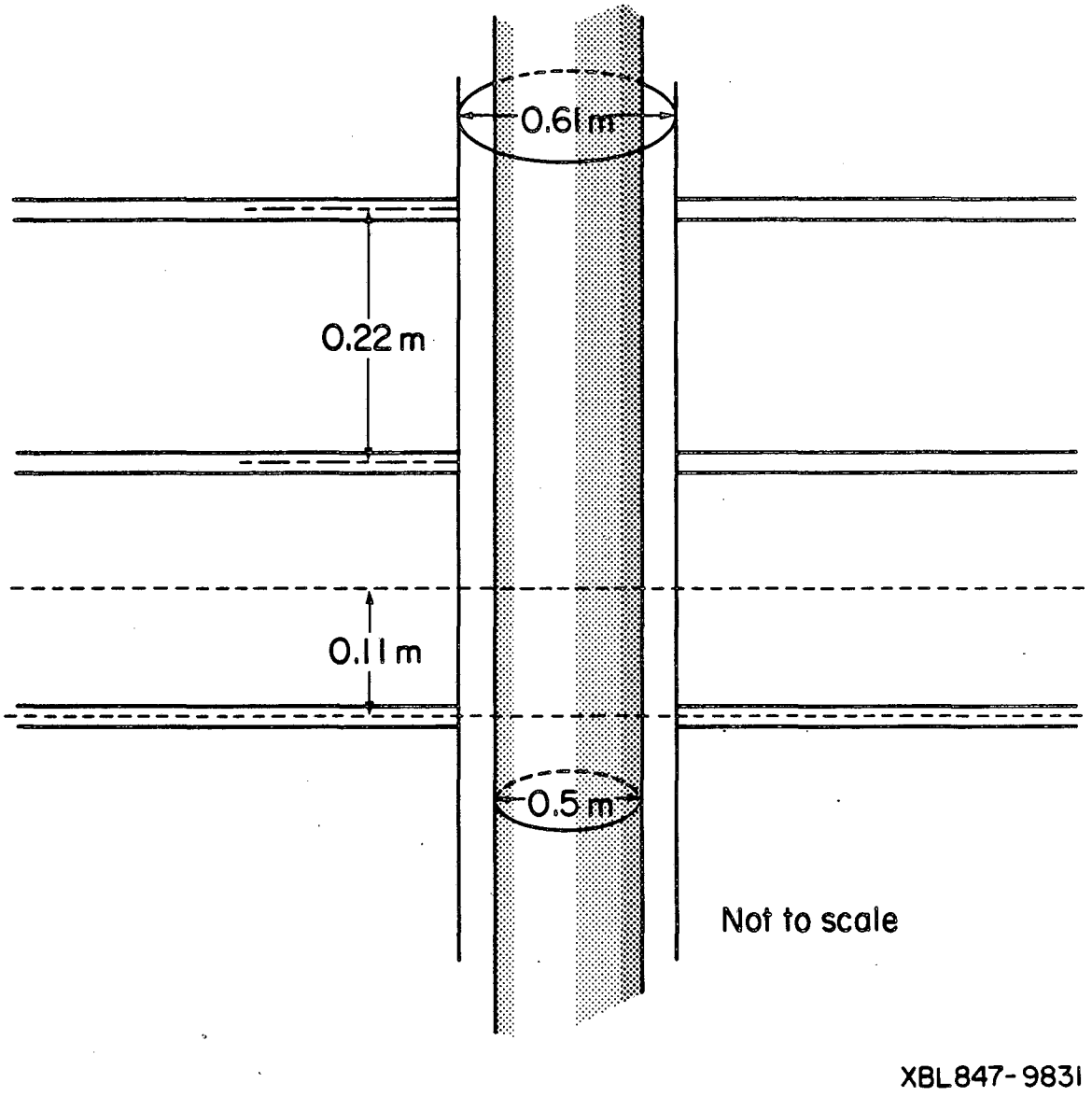

Figure 1. Idealized emplacement configuration. An infinite linear string of waste packages is intersected by fractures with 0.22 m spacing.

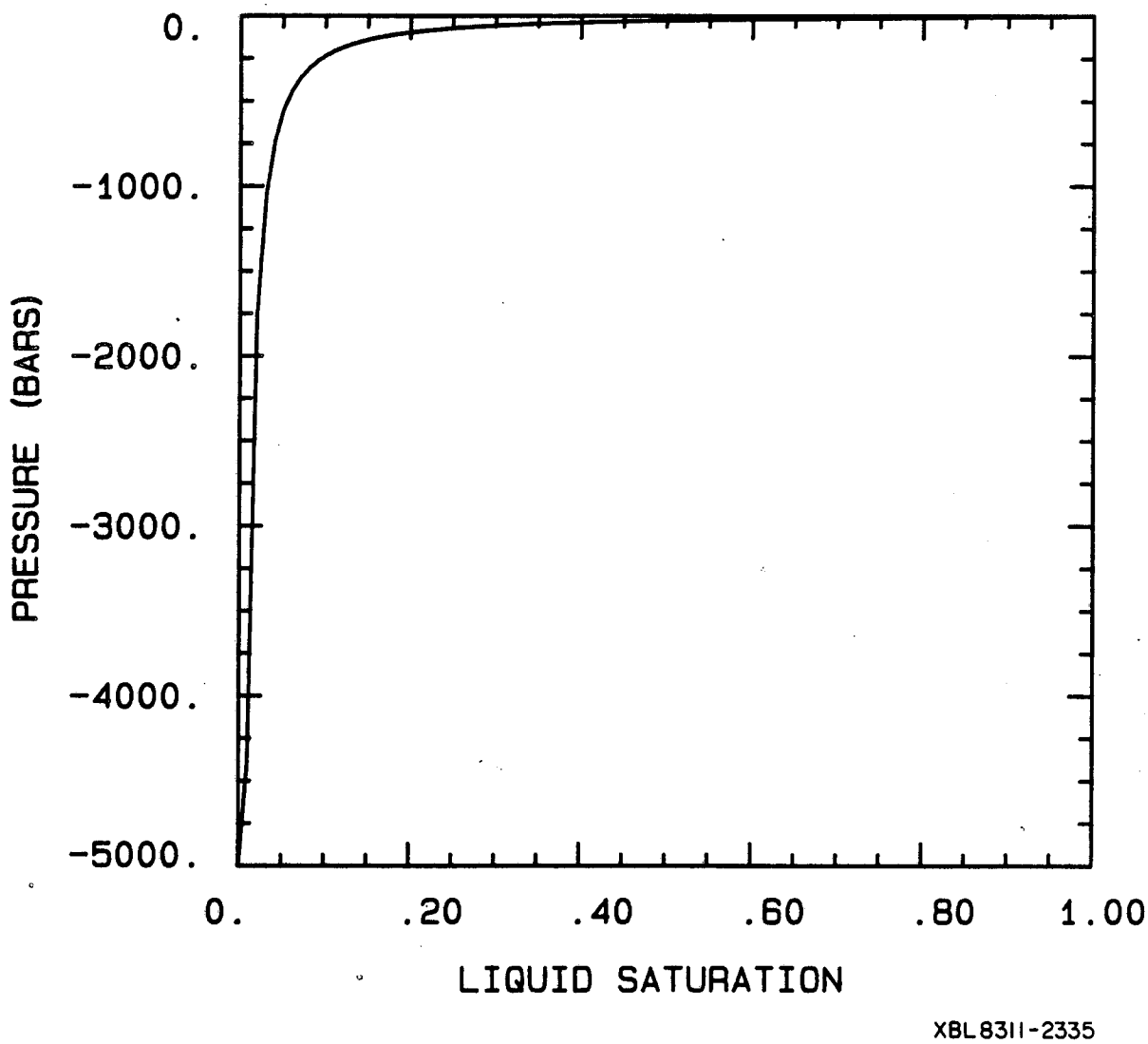

Figure 2. Suction pressure of tuff matrix.

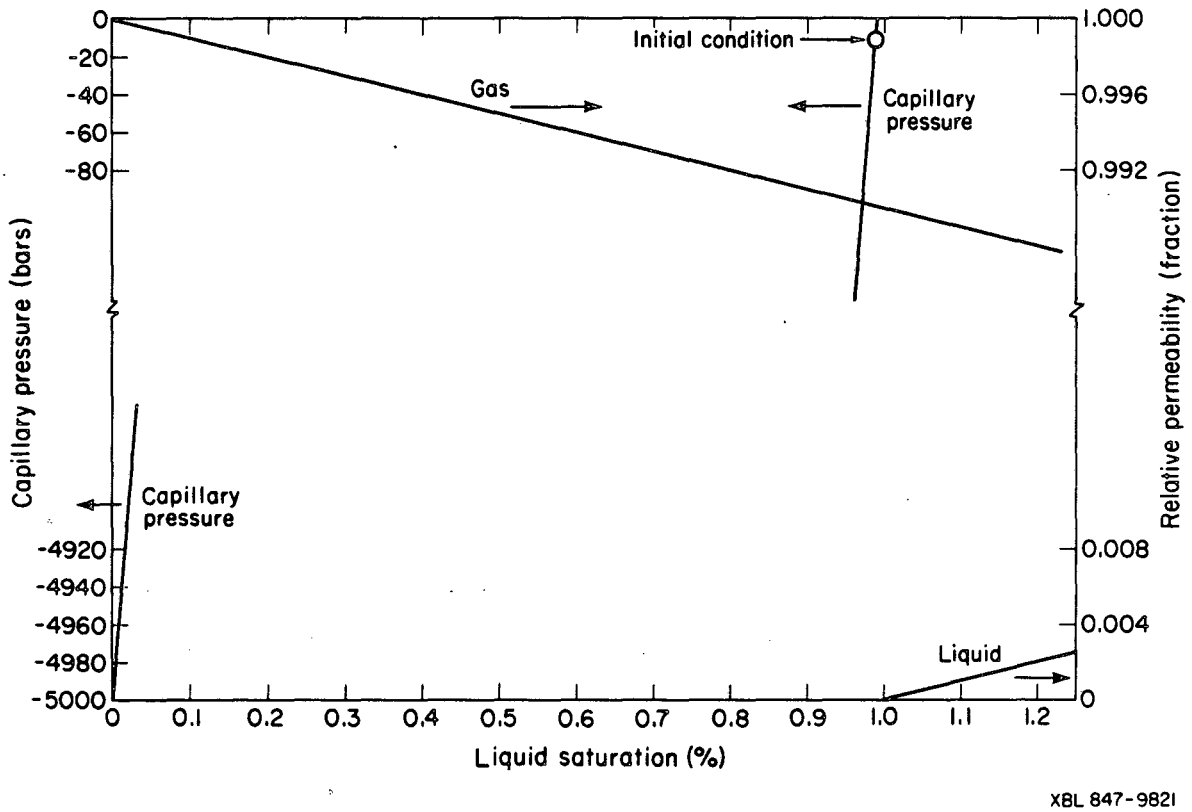

Figure 3. Hypothetical characteristic curves in the fractures (Case 1; liquid immobile in fractures).

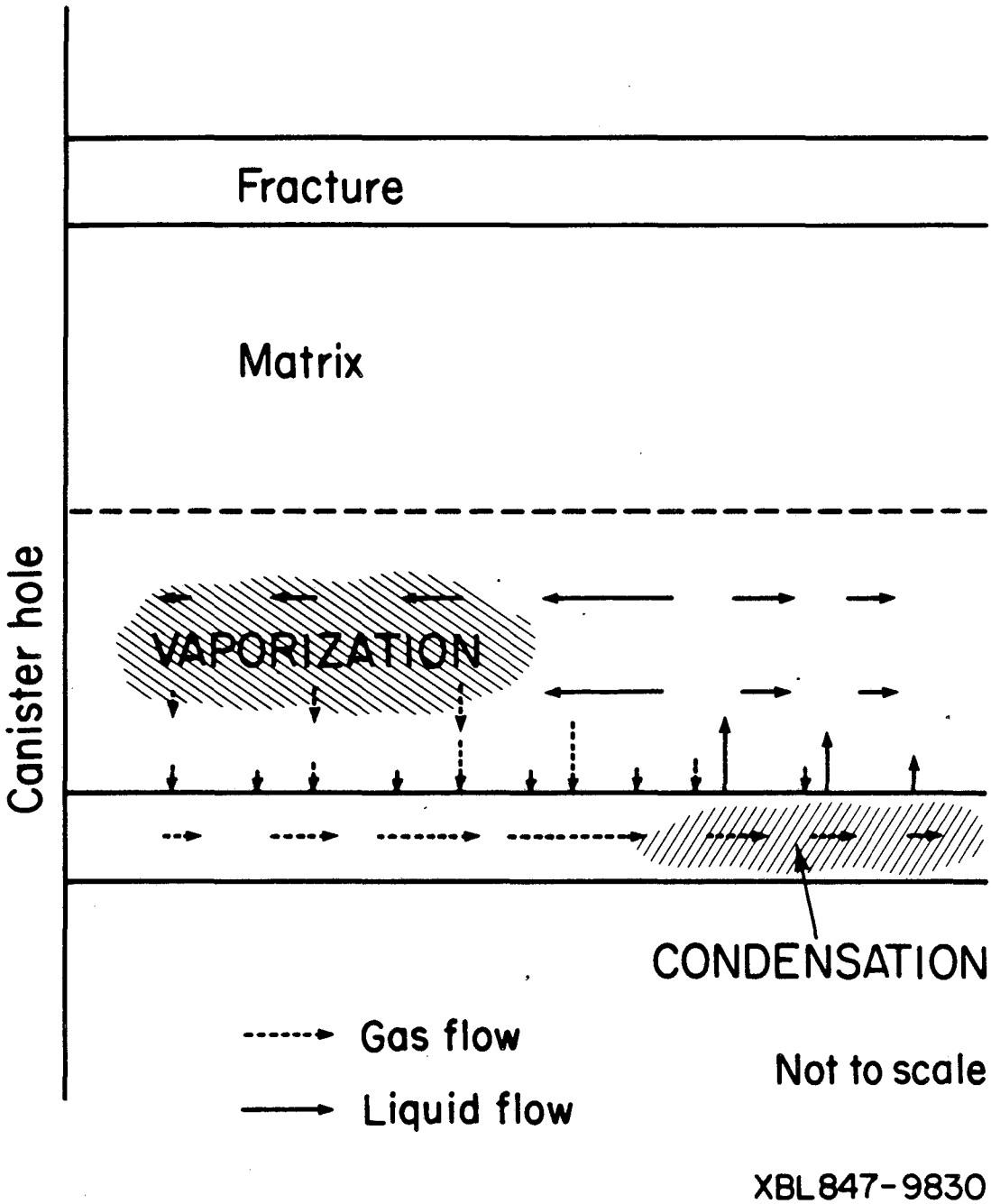

Figure 4. Response of fractured porous medium to heat load for case with immobile liquid in fractures.

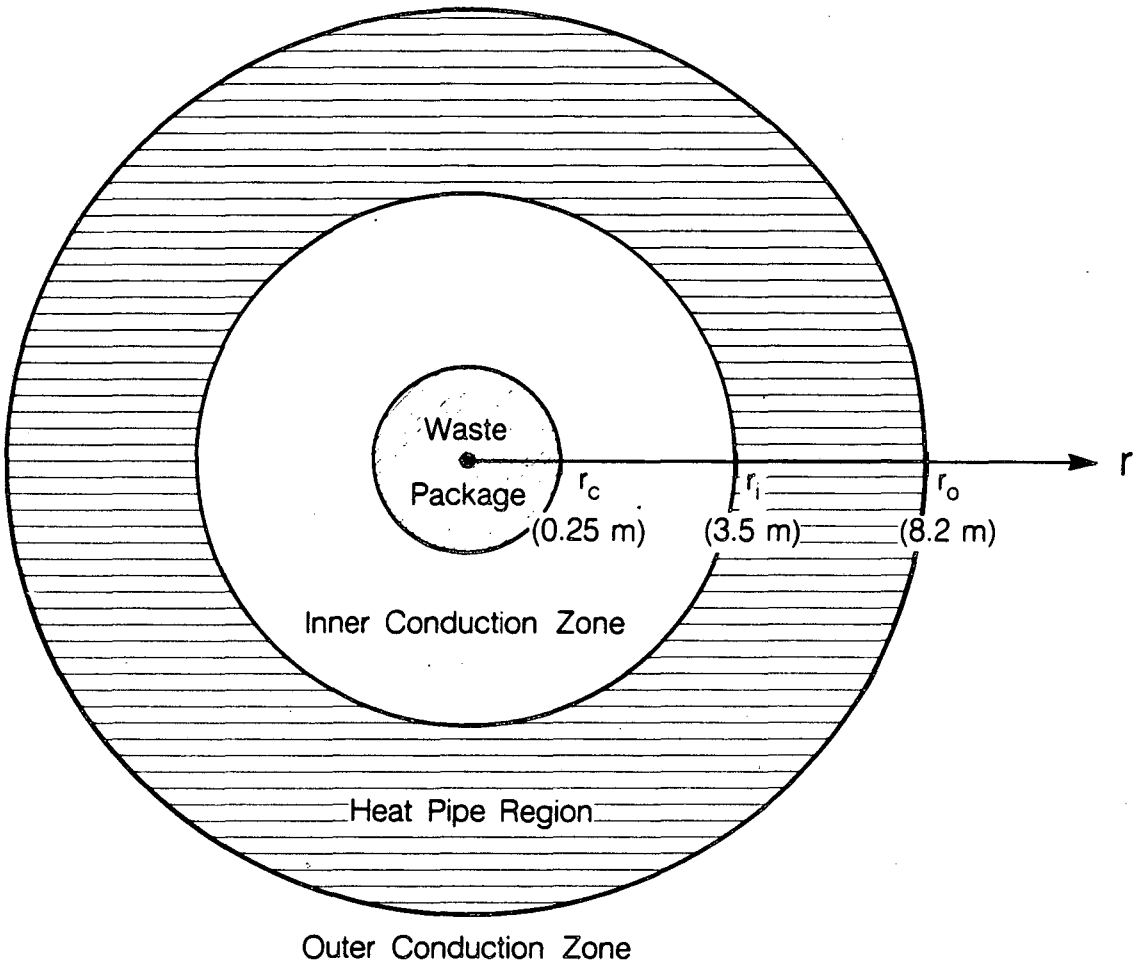

XBL 8511-12642

Figure 5. Schematic of thermohydrological regime in plane perpendicular to the axis of the waste packages (not to scale; the parameters of the heat pipe region correspond to a time of 26.89 yr after waste emplacement for backfilled conditions).

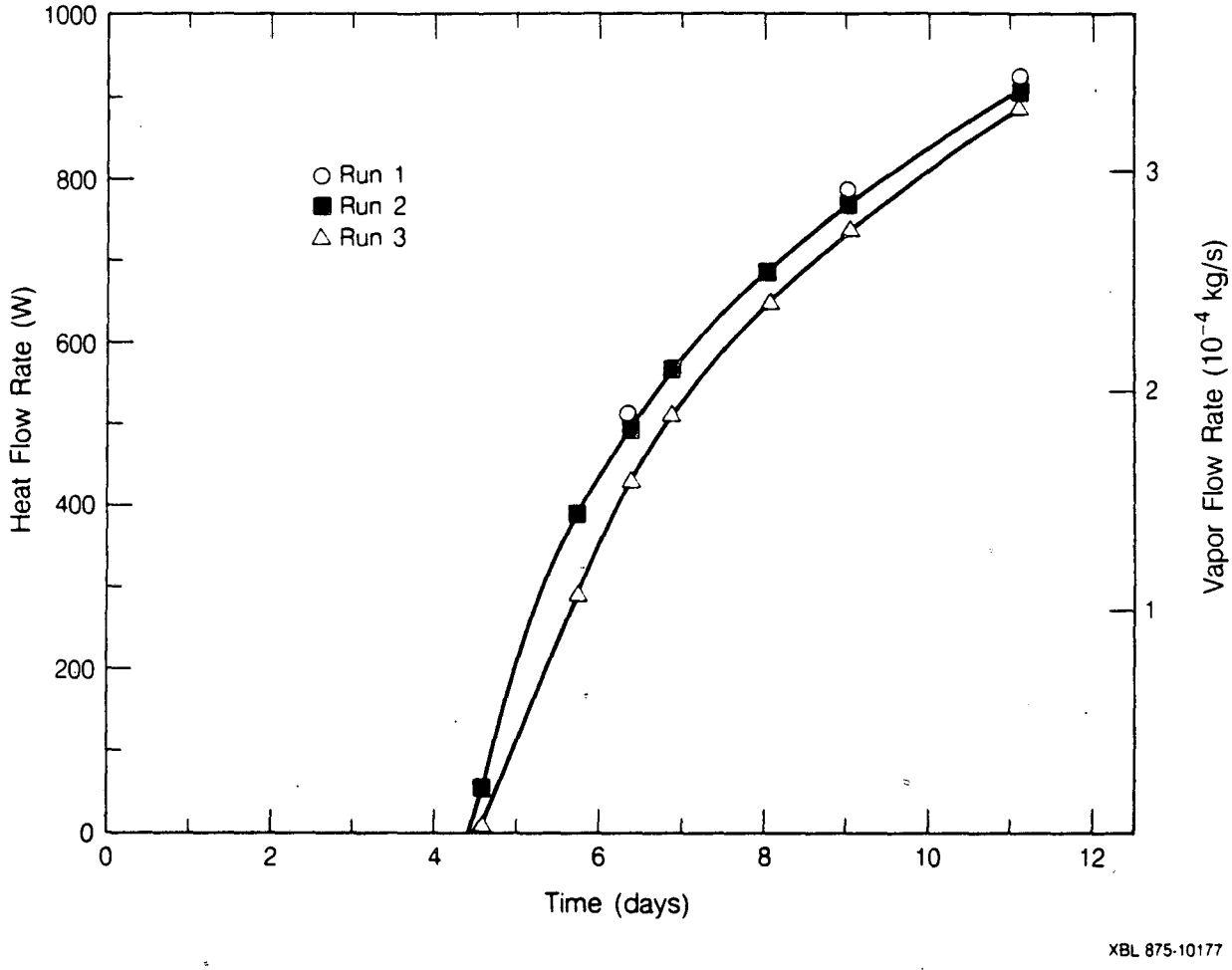

Figure 6. Heat and vapor flow rates from emplacement hole (open-hole conditions, liquid mobile in fractures).

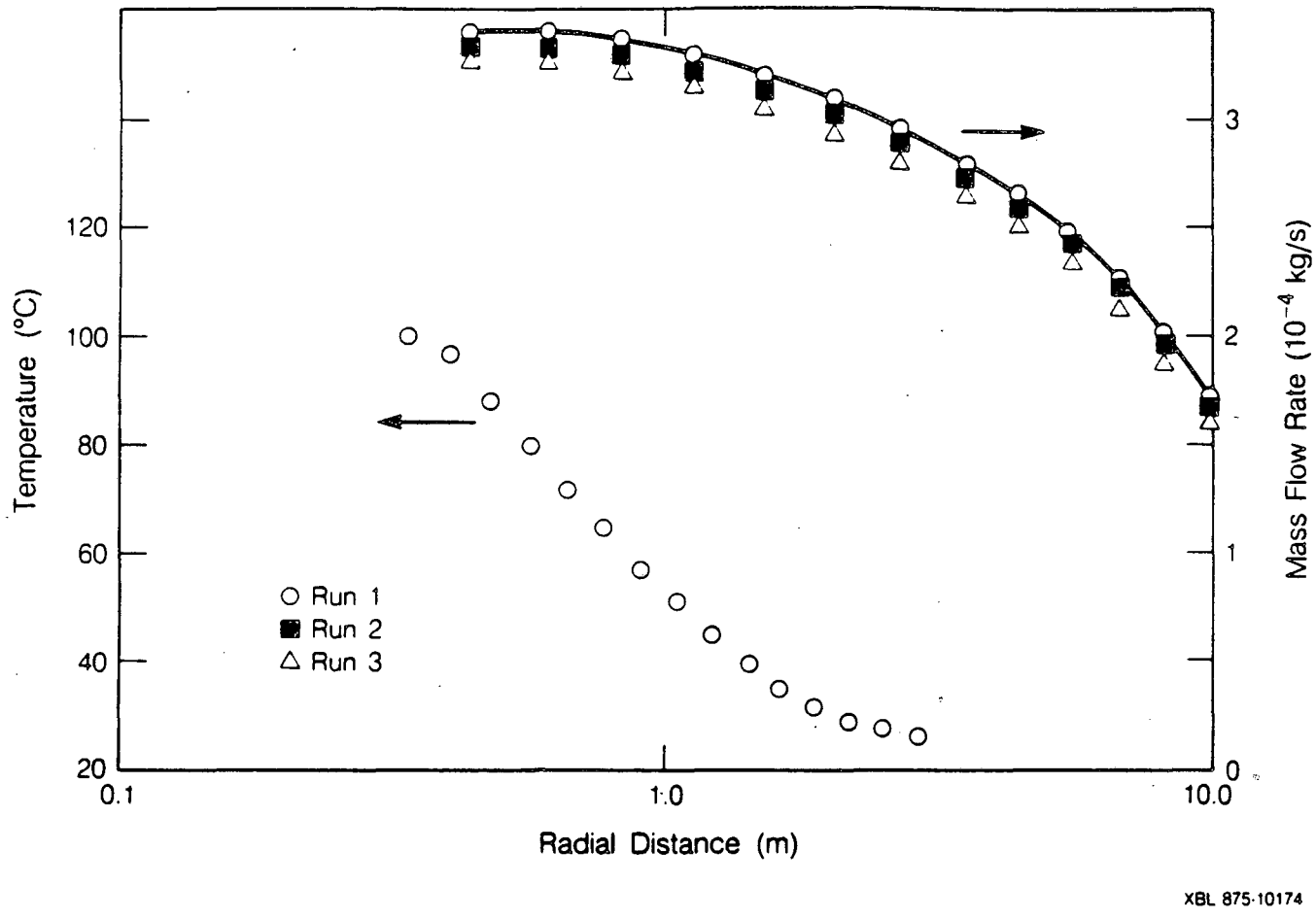

Figure 7. Temperature and liquid flow patterns at 11.1 days after waste emplacement (open-hole conditions, liquid mobile in fractures).

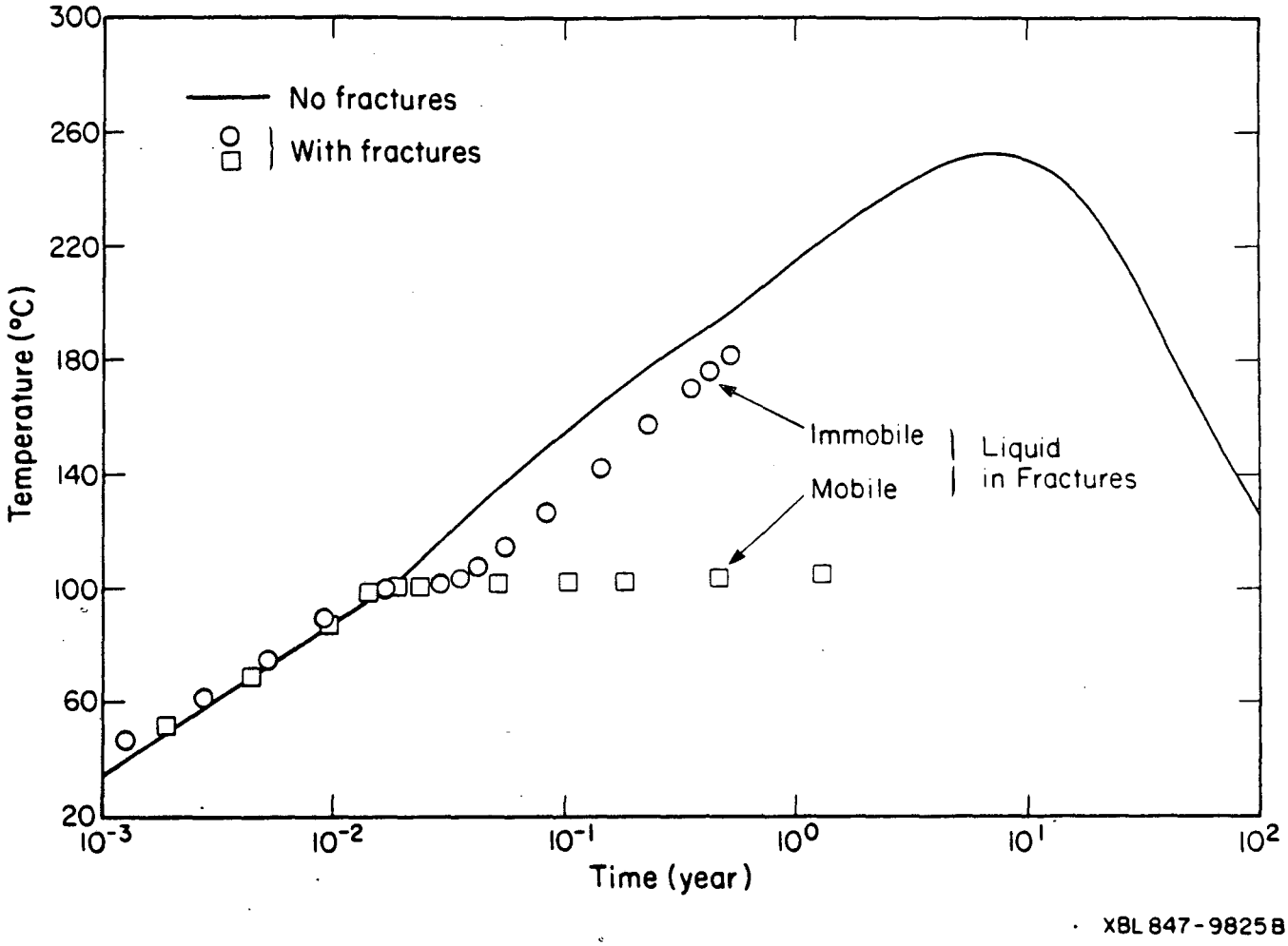

Figure 8. Simulated temperatures at a distance of 0.34 m from the centerline of the waste packages for backfilled emplacement conditions.

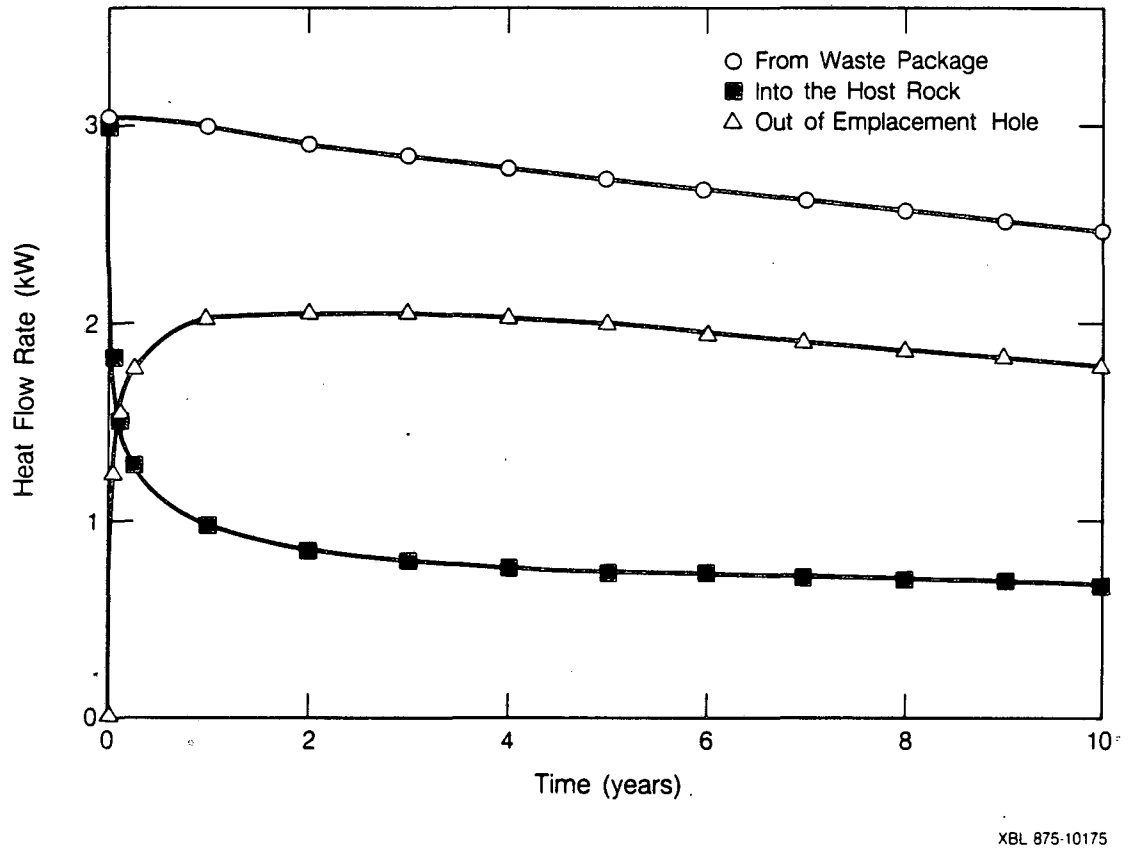

Figure 9. Heat flow rates for open hole emplacement, with liquid mobile in fractures.

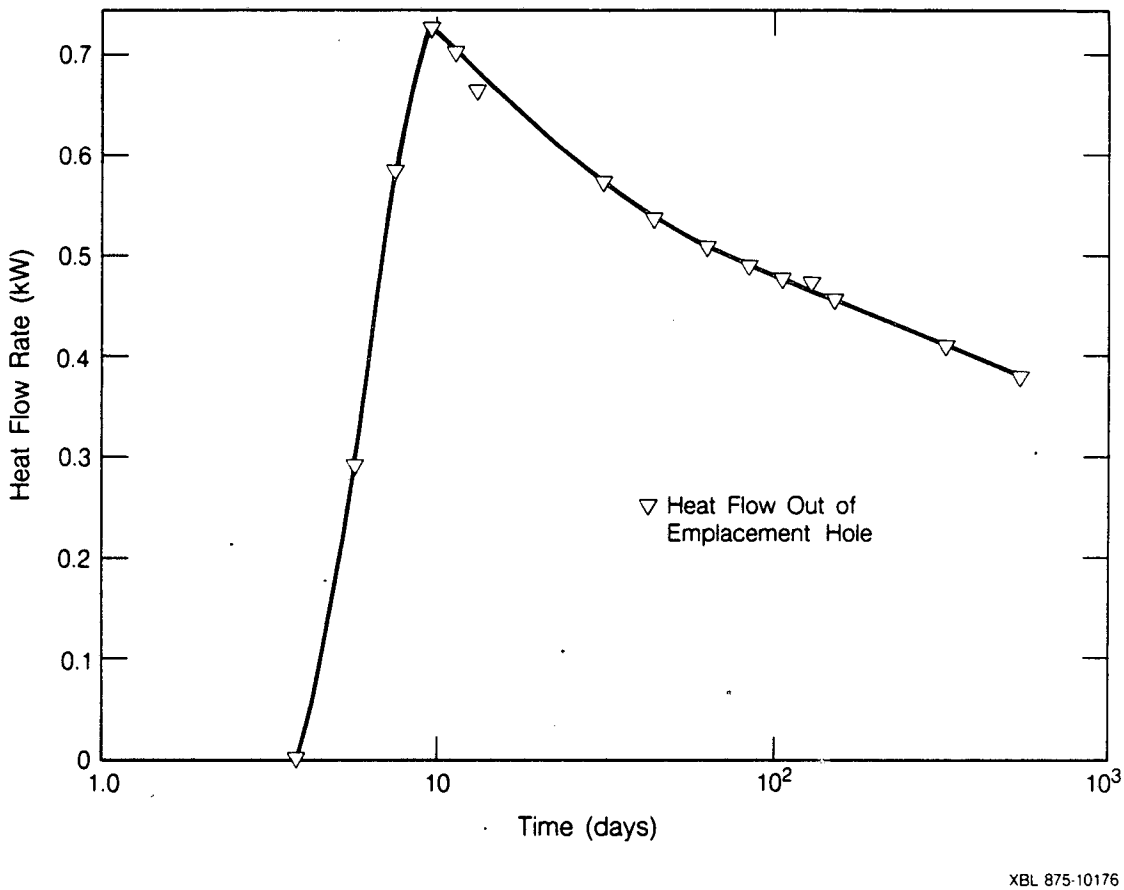

Figure 10. Heat loss from emplacement hole for case with immobile liquid in the fractures.

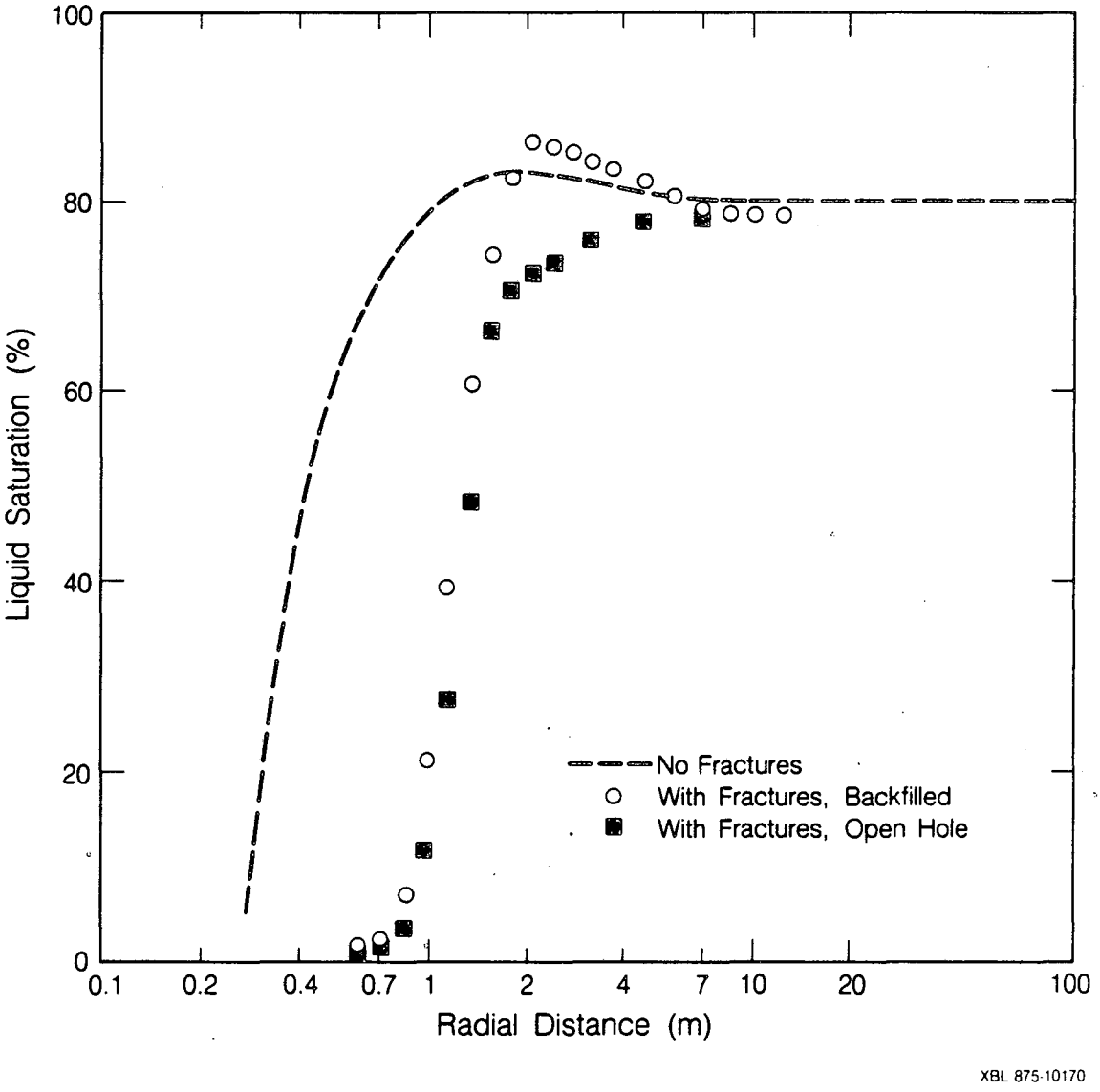

Figure 11. Liquid saturation distribution at 160 days after waste emplacement (liquid immobile in fractures).

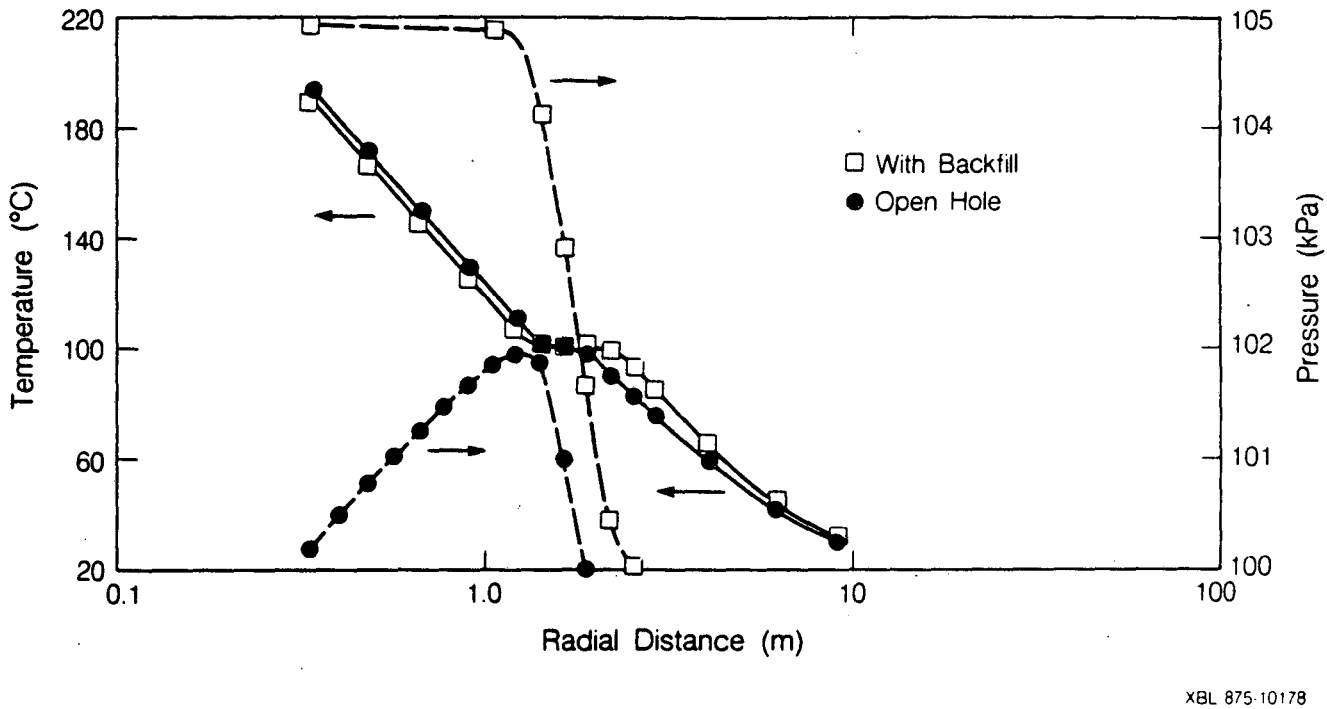

Figure 12. Temperatures and pressure at 264 days after waste emplacement for open-hole and backfilled conditions (liquid immobile in fractures).

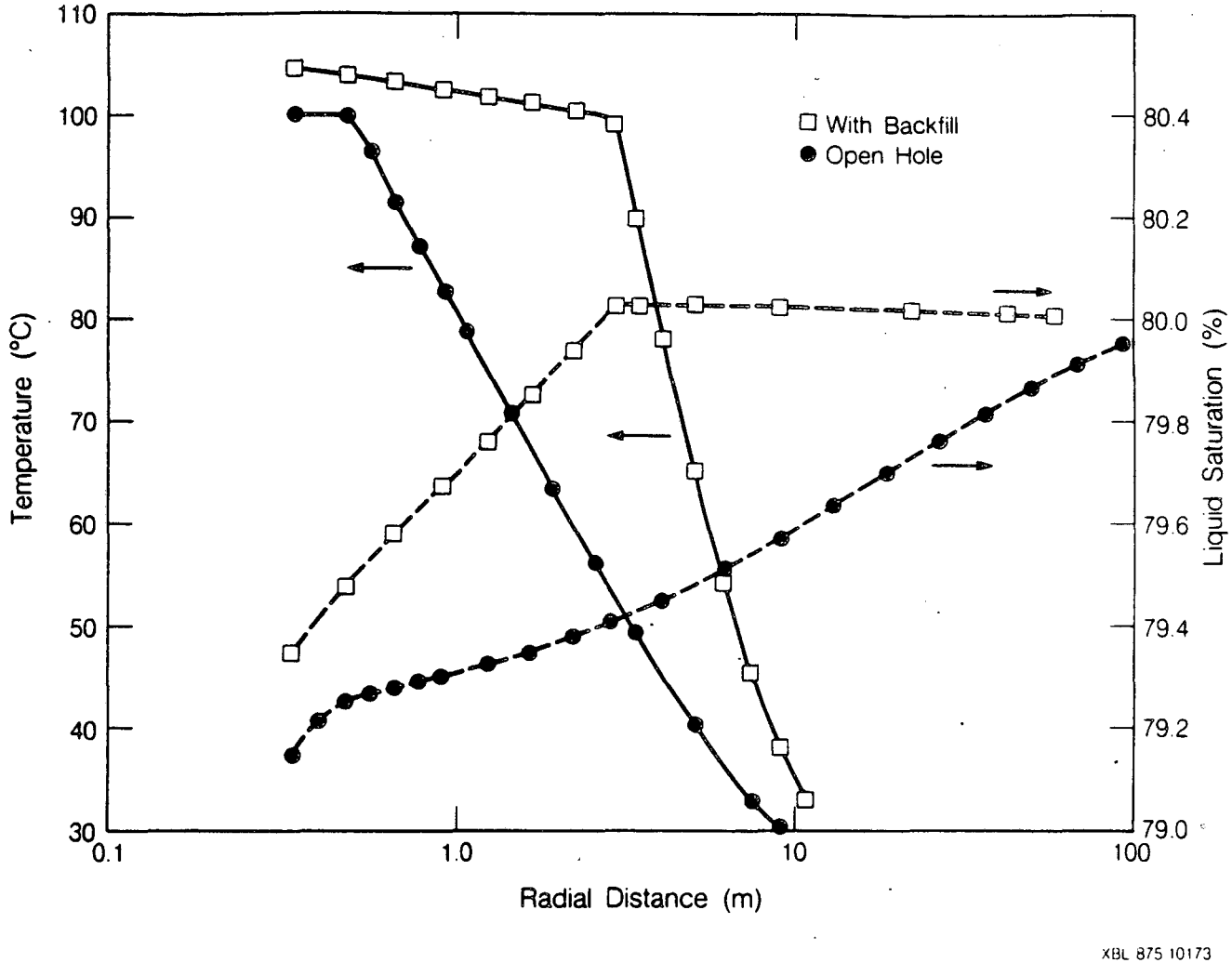

Figure 13. Temperatures and liquid saturations at 1 yr after waste emplacement for open-hole and backfilled conditions (liquid mobile in fractures).

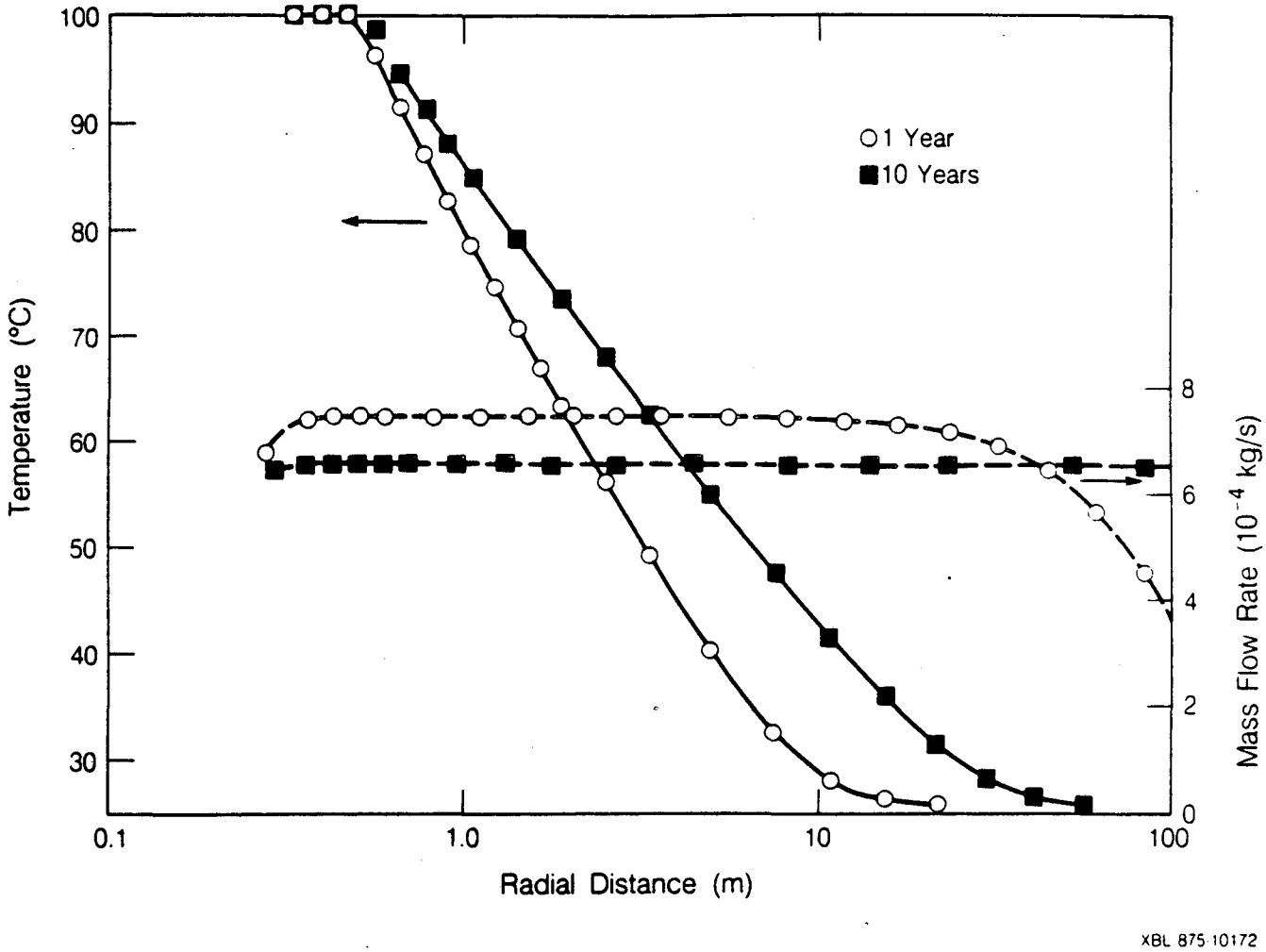

Figure 14. Temperature profiles at 1 and 10 yr after waste emplacement, and liquid flow rate in fractures (open hole, liquid mobile in fractures).

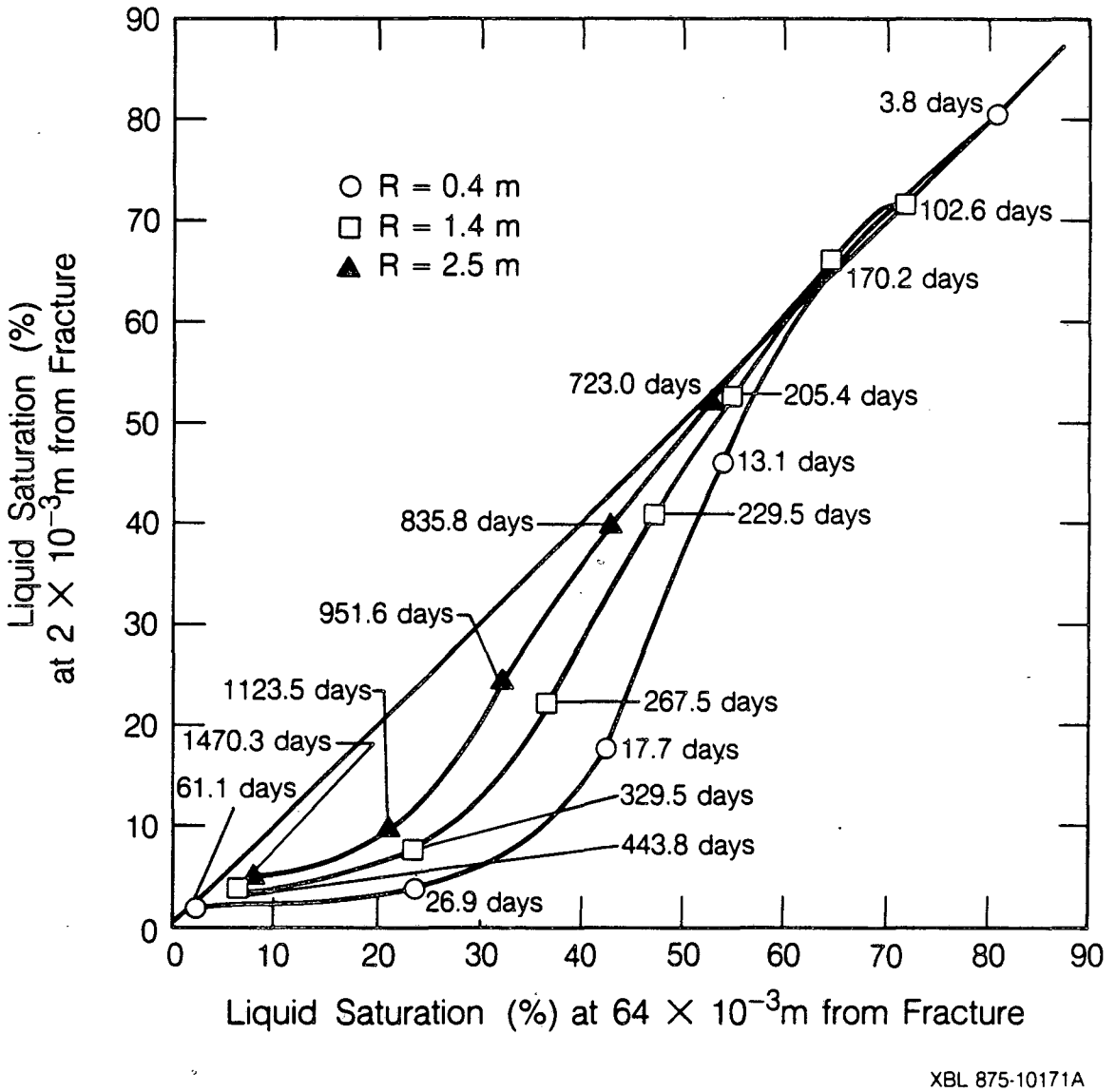

Figure 15. Drying trajectories for selected points in the rock matrix (open hole, liquid immobile in fractures). The times at which different saturations are reached are indicated.

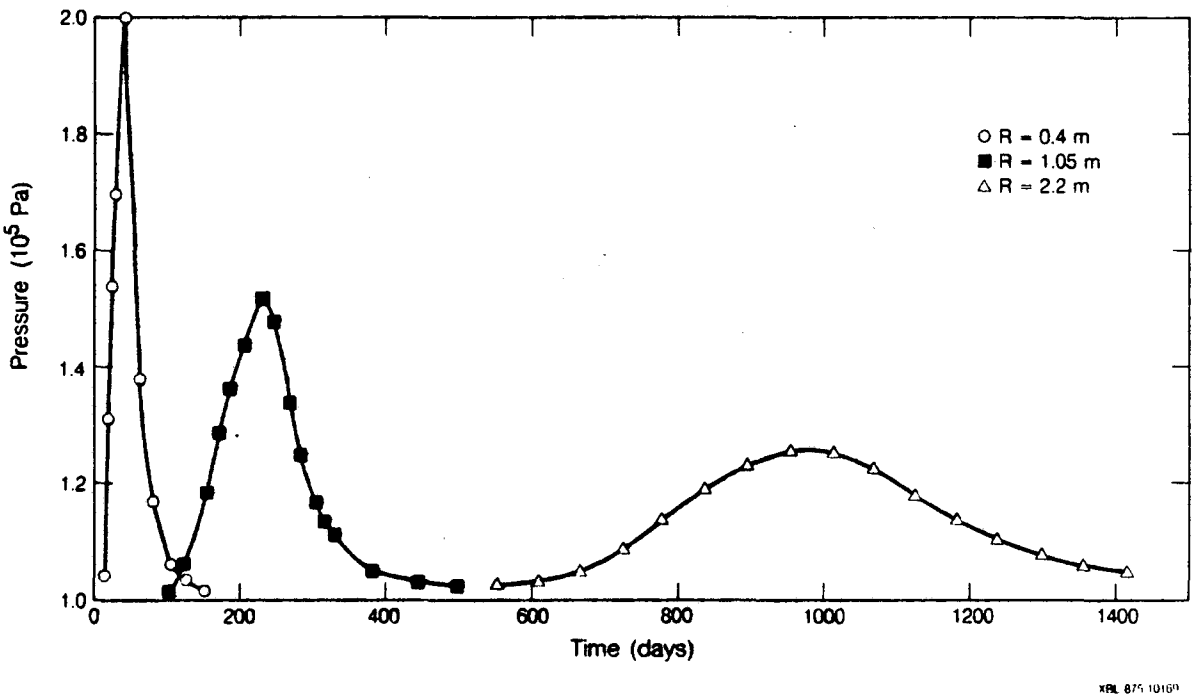

Figure 16. Pressure transients in the rock matrix at a distance of 64 mm from the fracture (open hole, liquid immobile in fractures).

LAWRENCE BERKELEY LABORATORY
TECHNICAL INFORMATION DEPARTMENT
1 CYCLOTRON ROAD
BERKELEY, CALIFORNIA 94720